NASA Contractor Report 4080

Heat Generation in Aircraft Tires Under Yawed Rolling Conditions

Richard N. Dodge and Samuel K. Clark

GRANT NSG-1607
JULY 1987

NASA

NASA Contractor Report 4080

Heat Generation in Aircraft Tires Under Yawed Rolling Conditions

Richard N. Dodge and Samuel K. Clark
The University of Michigan
Ann Arbor, Michigan

Prepared for
Langley Research Center
under Grant NSG-1607

National Aeronautics
and Space Administration

**Scientific and Technical
Information Office**

1987

SYMBOLS

English Letters

d	tire diameter
K	foundation stiffness
ℓ	patch length
p	pressure
q	rate of heat release per unit volume
T	string tension
w	tire width
W	work done

Greek Letters

α	yaw angle
β	series coefficient
δ	deflection
η	fractional part of lateral shift
τ	shear stress
μ	friction coefficient

Subscripts

L	inboard side of tire
R	outboard side of tire
o	initial
y	lateral
z	vertical

INTRODUCTION

An analytical theory allowing the calculation of internal temperature in free-rolling aircraft tires has been described previously in ref. [1]. That theory was based on estimating the stress changes in various portions of a tire as each portion rolled through the contact patch, and then using those changes to estimate the corresponding rate of heat release from known loss properties of the materials used in tire construction. The stress changes were obtained by treating the tire as a shell structure. Comparisons of calculations using this theory with experimental data taken from thermocouples imbedded in typical aircraft tires showed generally good agreement.

An extension of this work to the case of the tire under braking conditions has been described in a subsequent report, ref. [2]. That theory was based on the power loss due to hysteretic losses in the tire materials caused by stress cycling. Comparisons were again made between predictions using this theory and data taken on instrumented aircraft tires under braked rolling conditions.

The present report represents an extension of these two efforts to the case of the tire under yawed rolling conditions. It is shown that there are several mechanisms contributing to stress changes in both the tread and sidewall regions during cornering of a tire. These stress changes are used to estimate

the rate of heat generation at each point in the tire. This report presents an analytical background for the calculation of these changes and the subsequent heat generated. Comparisons are again made between predictions using this analysis and data taken on instrumented aircraft tires.

ANALYTICAL DEVELOPMENT

In ref. [1] a method has been developed for calculating the internal temperature distribution in an aircraft tire while free rolling under load. The method uses an approximate stress analysis of each point in the tire as it rolls through the contact patch, and from this stress change the mechanical work done on each volume element may be obtained and converted into a heat release rate through a knowledge of material characteristics. The tire cross-section is then considered as a body with internal heat generation, and the heat diffusion equation is solved numerically with appropriate boundary conditions at the tire surface.

The extension of this analysis to the aircraft tire under yawed rolling conditions is based on the same major assumptions used for the free rolling tire, mainly that the change in strain is based on

(a) The fact that the tire is made up of a series of material points, each of which undergoes a change in stress state as it moves from A to B as shown in Figure 1, and

(b) that in calculating the strain energy at either point A or B, the cross-section of the tire may be represented geometrically by its neutral axis, around which act both membrane and bending strains.

In the present analysis the portion of the tire tread in contact with the runway or drum surface is assumed to take

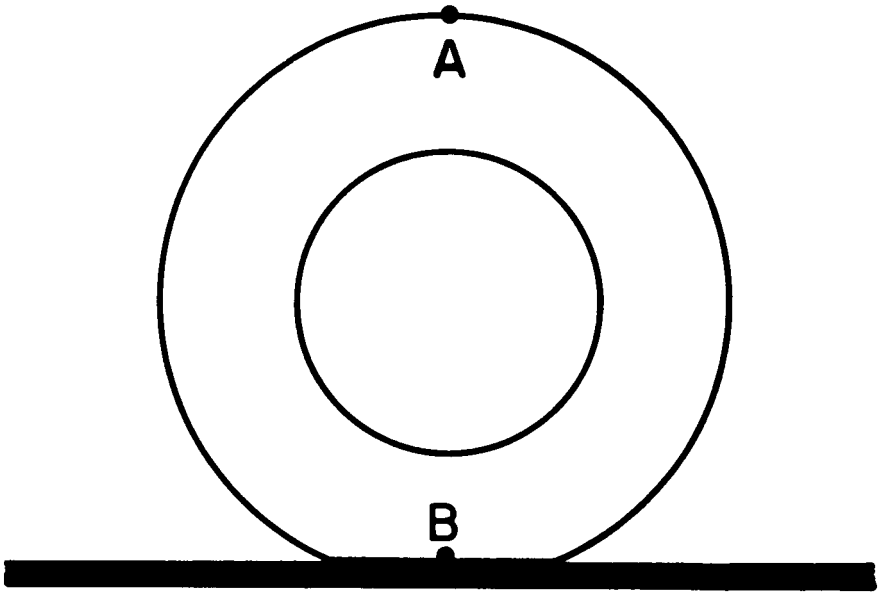

Fig. 1. Extreme points of stress excursion in a tire.

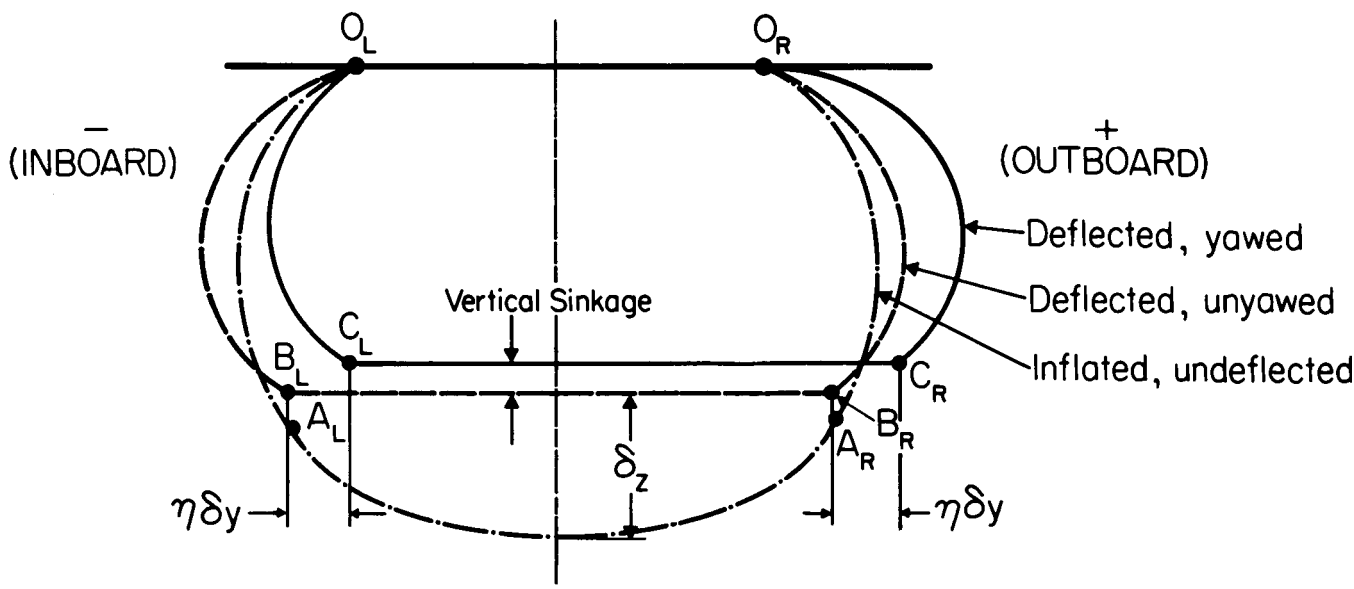

Fig. 2. Assumed geometry, before and after deformation.

the curvature of that surface, while the sidewall out of contact is approximated by using a segment of a circular arc. However, unlike the free rolling case, the yawed rolling conditions generate a meridianal cross-section which is no longer symmetrical in the deformed state at position B. This is illustrated in Figure 2 where it is noted that "Outboard or (+)" side of the tire refers to the right side as viewed from the front, assuming the tire is rolling out of the page and has been yawed to the right (counterclockwise yaw angle as viewed from above).

Heat generation in the tire during cornering arises in three ways:

(a) Heat generated from cyclic stress changes as described in ref. [1]. These changes will be different for the inboard and outboard region of the cross-section due to the unsymmetrical geometry changes.

(b) Heat generated at the interface between the tire and runway due to physical sliding of the tread rubber against the runway. A fraction of this heat flows into the tread surface and a fraction into the runway.

(c) Heat generated in the tread elements due to cyclic shear forces.

Each of these forms will be analyzed in order.

The detailed description of the heat generated from cyclic stress changes in ref. [1] requires the determination of the curvature of the meridianal cross-section at positions A and B of

Figure 1. The idealized cross-section at position A is represented by the arcs $O_L A_L, A_L A_R, A_R O_R$. These are assumed to be segments of circular arcs as discussed in Appendix B of ref. [1]. The idealized cross-section at position B can be envisioned as a symmetrical unyawed deflection represented by arcs $O_L B_L, B_L B_R, B_R O_R$ followd by an unsymmetrical lateral shift due to the cornering action. This is represented by $O_L C_L$, $C_L C_R$, $C_R O_R$.

The calculation of this final geometry requires the determination of the points C_L and C_R from the vertical deflection δ_z and the yaw angle α. Referring to Figure 2, the ordinate of C_L and C_R is:

$$Y_{C_L} = Y_{C_R} = Y_B - \delta_z - .2\delta_y \tag{1}$$

where δ_y is the lateral shift of the centerline and $0.2\delta_y$ is the approximate vertical sinkage due to the cornering action, see ref. [3].

Due to the kinematics of the lateral deformation, points C_L and C_R only move a fraction of the lateral shift δ_y. Thus the abscissa of C_L and C_R are:

$$\begin{aligned} X_{C_L} &= X_B - \eta\delta_y \\ X_{C_R} &= X_B - \eta\delta_y \end{aligned} \tag{2}$$

where $0 \leq \eta \leq 1$.

It has also been observed from slow-rolling action of yawed tire models against a curved drum surface that extra material appears to "roll" into the outboard side while material appears to "roll" out of the inboard side. Thus the sidewall arcs are:

$$O_L C_L = O_L A_L - \eta\delta_y$$
$$O_R C_R = O_R A_R + \eta\delta_y \qquad (3)$$

The determination of X_B and Y_B in equations (1) and (2) follow the same details outlined in ref. [1]. Therefore to determine the coordinates of C_L and C_R only requires the calculation of δ_y and an evaluation of η. A value of $\eta = 0.5$ was used in the calculations of this report. The lateral deflection of the center of contact, δ_y, is analyzed by using a string-type model discussed below.

The lateral motion of the tire centerline is determined by taking a unit width of tread at a slip angle α, friction coefficient μ, and contact pressure $p(x,0)$ in the contact patch, as shown in Figure 3. It is assumed that the tire does not slip with respect to the ground plane until the point x_1 is reached.

At x_1 the elastic forces of the tire overcome the retarding frictional forces and from A to B the tire slips back to the wheel plane, reaching its equilibrium position at the end of the contact patch where $x = \ell$. Thus δ_y is represented by the value of y at x_1.

It is assumed that the pressure distribution is sinusoidal:

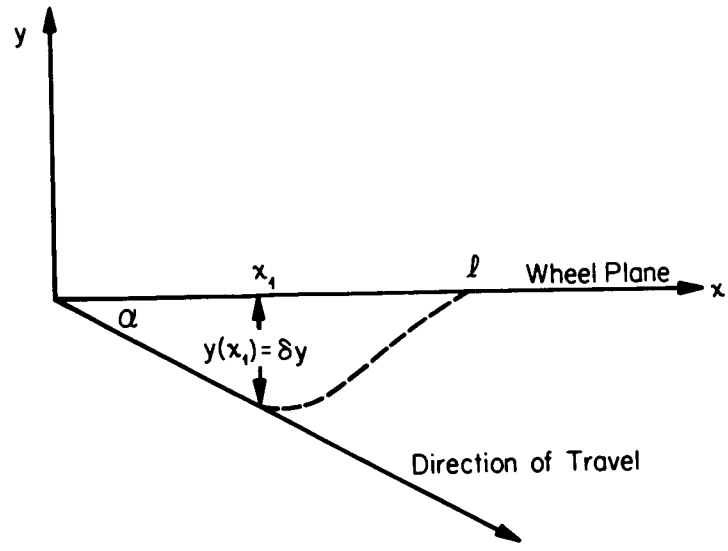

Fig. 3. Idealized slip path of contact patch centerline.

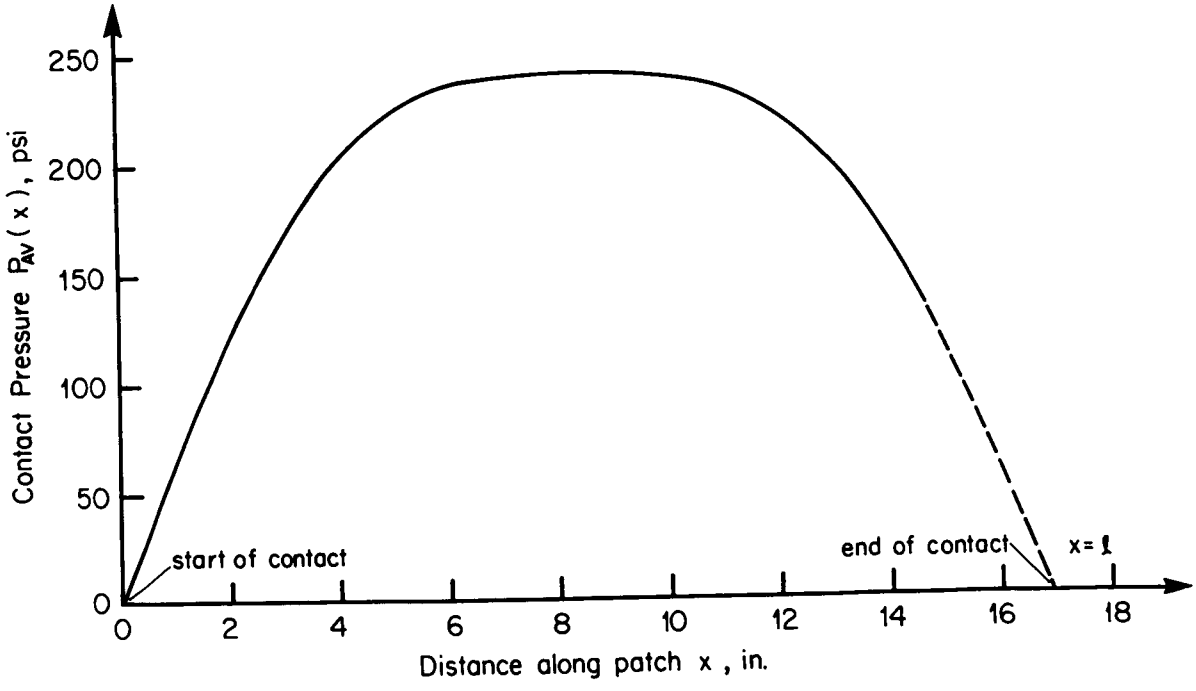

Fig. 4. Predicted pressure distribution from equation (4) for a 40x14/22 PR aircraft tire with an inflation pressure of 175 psi and a vertical deflection of 2.66 in.

$$P_{av}(X) = \frac{\pi P_o}{2(1-\frac{\beta}{3})}\left[\sin(\frac{\pi x}{\ell}) - \beta\sin(\frac{3\pi x}{\ell})\right] \qquad (4)$$

where P_o = inflation pressure, $\beta = -0.25$, and

$$\ell = 2[0.85\sqrt{\delta_z d_o - \delta_z^2}] \quad , \text{ from ref.[3].}$$

A typical pressure distribution predicted from equation (4) for a 40x14/22 PR aircraft tire is shown in Figure 4.

Using a string model for the tire

$$T\frac{d^2y}{dx^2} - Ky = q(X) \qquad (5)$$

where $q(X)$ = tangential shear stress = $\mu P_{av}(X)$

K = foundation stiffness per unit length, lb/in/in

T = string tension, lbs.

In the region $0<X<X_1$

$$Y = -X \tan\alpha \qquad (6)$$

The limiting condition is reached when (if the curvature $\simeq 0$) $-Ky_1 = \mu p(x)$, or using eq. (4) and (6)

$$Kx_1\tan\alpha = \frac{\mu\pi P_o}{2(1-\beta/3)}\left[\sin(\frac{\pi X_1}{\ell}) - \beta\sin(\frac{3\pi X_1}{\ell})\right] \qquad (7)$$

Equation (7) can be used to solve for X_1 and using eq. (6),

$$\delta_y = X_1 \tan\alpha \qquad (8)$$

The necessary geometry calculations can now be completed in eqs. (1), (2), and (3), and from these results, and the analysis developed in ref. [1], calculations can be completed for the heat generated from cyclic stress changes. However, since the geometry of deformation is no longer symmetrical, this

analysis will need to be used separately for the inboard and outboard regions of the tire.

The string model illustrated in Figure 3 can also be used to calculate the heat generated between the runway and the tire due to the physical sliding of the tread rubber against the runway.

Again referring to Figure 3, for $x>x_1$ the equation governing y is:

$$T\ \frac{d^2y}{dX^2} - Ky = C \sin\left(\frac{\pi X}{\ell}\right) + D \sin\left(\frac{3\pi X}{\ell}\right) \tag{9}$$

where

$$C = \frac{\mu\pi P_o}{2(1-\beta/3)} \quad \text{and} \quad D = -\beta C$$

The solution to (9) is:

$$Y = Ae^{-\lambda x} + Be^{\lambda x} - C_1 \sin\left(\frac{\pi x}{\ell}\right) - D_1 \sin\left(\frac{3\pi x}{\ell}\right) \tag{10}$$

where

$$\lambda^2 = \frac{K}{T}, \quad C_1 = \frac{C}{K+\frac{\pi^2 T}{\ell^2}}, \quad D_1 = \frac{D}{K + \frac{9\pi^2 T}{\ell^2}}$$

Equation (10) is subject to the boundary conditions:

$$Y(X_1) = -X_1 \tan\alpha \tag{11}$$

$$Y(\ell) = 0 \tag{12}$$

Using eqs. (11) and (12) in Eq. (10) gives:

$$B = \frac{C_1 \sin\left(\frac{\pi X_1}{\ell}\right) + D_1 \sin\left(\frac{3\pi X_1}{\ell}\right) - X_1 \tan\alpha}{e^{\lambda x_1} - e^{\lambda(2\ell - x_1)}} \tag{13}$$

$$A = -B\, e^{2\lambda\ell} \tag{14}$$

The scrubbing work is the product of the tangential pressure and slip distance at each location, i.e.,

$$W = \int q \, dy \tag{15}$$

Recalling that $q = \mu p(x) = C \sin(\frac{\pi x}{\ell}) + D \sin(\frac{3\pi x}{\ell})$, and using eq. (10).

$$dy = [-\lambda A e^{-\lambda x} + \lambda B e^{\lambda x} - C_1 (\frac{\pi}{\ell}) \cos(\frac{\pi x}{\ell}) - D_1 (\frac{3\pi}{\ell}) \cos(\frac{3\pi x}{\ell})] \tag{16}$$

Substituting eq. (16) into eq. (15) and integrating over that portion of the patch length where slipping takes place, i.e., from x_1 to ℓ gives:

$$W = \sum_{I=1}^{8} WI \tag{17}$$

where

$$W1 = \frac{-\lambda AC}{(\lambda^2 + \frac{\pi^2}{\ell^2})} [(\frac{\pi}{\ell}) \bar{e}^{\lambda \ell} + (\lambda \sin(\frac{\pi x_1}{\ell}) + (\frac{\pi}{\ell}) \cos(\frac{\pi x_1}{\ell})) \bar{e}^{\lambda x_1}] \tag{18}$$

$$W2 = \frac{-\lambda AD}{(\lambda^2 + \frac{9\pi^2}{\ell^2})} [(\frac{3\pi}{\ell}) e^{-\lambda \ell} + (\lambda \sin(\frac{3\pi x_1}{\ell}) + (\frac{3\pi}{\ell}) \cos(\frac{3\pi x_1}{\ell})) \bar{e}^{\lambda x_1}] \tag{19}$$

$$W3 = \frac{\lambda BC}{(\lambda^2 + \frac{\pi^2}{\ell^2})} [(\frac{\pi}{\ell}) e^{\lambda \ell} - (\lambda \sin(\frac{\pi x_1}{\ell}) - (\frac{\pi}{\ell}) \cos(\frac{\pi x_1}{\ell})) e^{\lambda x_1}] \tag{20}$$

$$W4 = \frac{\lambda BD}{(\lambda^2 + \frac{9\pi^2}{\ell^2})^2} [(\frac{3\pi}{\ell}) e^{\lambda \ell} - (\lambda \sin(\frac{3\pi x_1}{\ell}) - (\frac{3\pi}{\ell}) \cos(\frac{3\pi x_1}{\ell})) e^{\lambda x_1}] \tag{21}$$

$$W5 = \frac{-C_1 C}{4} [\cos(\frac{2\pi x_1}{\ell}) - 1] \tag{22}$$

$$W6 = \frac{-DC_1}{8}\left[2\cos\left(\frac{2\pi x_1}{\ell}\right) + \cos\left(\frac{4\pi x_1}{\ell}\right) - 3\right] \tag{23}$$

$$W7 = \frac{-3CD_1}{8}\left[-2\cos\left(\frac{2\pi x_1}{\ell}\right) + \cos\left(\frac{4\pi x_1}{\ell}\right) + 1\right] \tag{24}$$

$$W8 = \frac{-D\,D_1}{4}\left[\cos\left(\frac{6\pi x_1}{\ell}\right) - 1\right] \tag{25}$$

The work W due to frictional sliding in eq. (17) is assumed to be distributed uniformly over the outer surface tread elements. For each unit of tread element surface area, the rate of heat generation is given by, (see ref. 1)

$$\dot{q} = .01\ U\ v_o/(r_o - \delta_z/3) \tag{26}$$

where $U = W/t$, v_o = forward speed, t = thickness of outside element.

The evaluation of $\dot{q}$ represents the heat generated due to the physical sliding of the tire against the runway surface.

However, this quantity still requires the calculation of K and λ.

From ref. [3], equation (33), the lateral spring rate of the whole tire is given by:

$$K_y = 2\ w(p + 0.24\ p_r)\left(1 - .7\ \frac{\delta_z}{w}\right) \tag{27}$$

where w = width of cross-section, δ_z = vertical deflection, p_r = rated inflation pressure.

In terms of string theory this is obtained by displacing the contact patch of length ℓ through a lateral displacement δ using a force F_y, see Figure 5. Using one-half of the total tire,

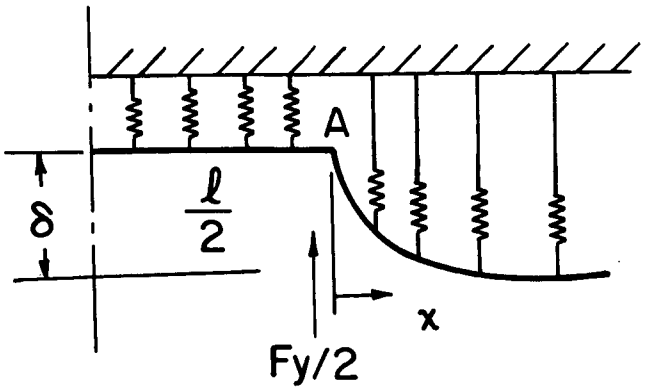

Fig. 5. Illustration of displacing contact patch through a lateral displacement in terms of string theory.

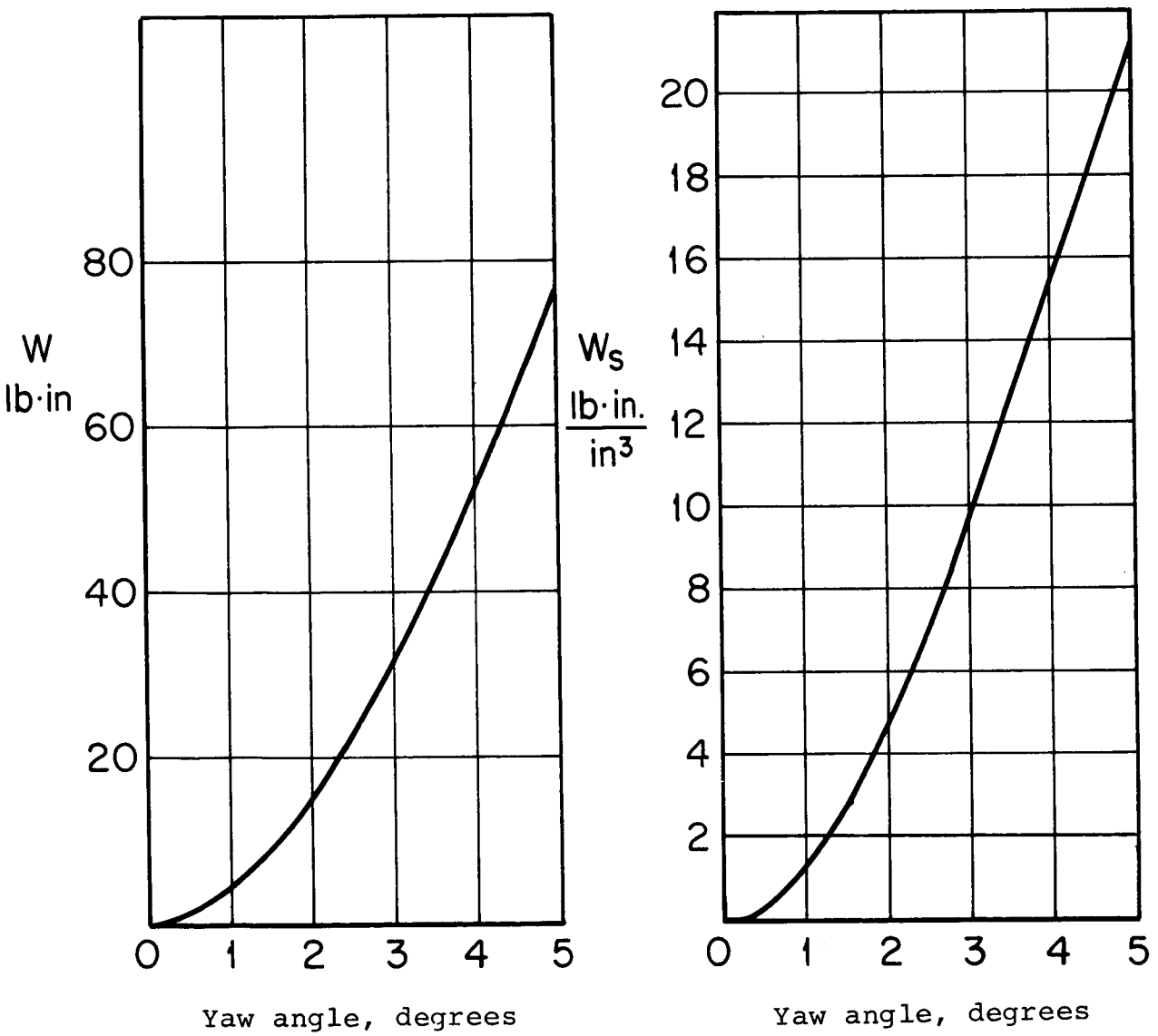

Fig. 6. Variation of scrubbing energy and cyclic shear stress energy loss with yaw angle.

and noting that at point A the string is free of loads so that

$$T \frac{d^2y}{dx^2} - Ky = 0$$

The solution to the string equation becomes

$$y = -\delta e^{-\lambda x} \quad \text{and} \quad \left(\frac{dy}{dx}\right)_{x=o} = \lambda\delta$$

Therefore,

$$\frac{Fy}{2} = K \frac{\delta\ell}{2} + T \left(\frac{dy}{dx}\right)_{x=o} = K \frac{\delta\ell}{2} + T\lambda\delta, \quad \text{and}$$

$$K_y = \frac{(Fy/2)}{\delta} + K\ell + 2T\lambda = K\ell + 2\sqrt{KT} \tag{28}$$

Also from ref. [3], λ is measured in terms of the lateral relaxation length so that

$$L_s = 1/\lambda \quad \text{and} \quad L_s/2w \simeq 0.6 \tag{29}$$

Thus

$$\lambda = 1/1.2w$$

However, since $\lambda^2 = K/T$, $T = 1.44\ w^2K$. Substituting into eq. (28) and solving for K gives

$$K = \frac{K_y}{\ell + 2.4\ w} \tag{30}$$

Thus from eqs. (27) and (30) K can be calculated from given geometry and operating conditions.

The final contribution to the heat generated due to cornering comes from the tread elements undergoing cyclic shear forces. Referring to Figure 1, each tread element experiences no shear

stress at position A and is subjected to the maximum tangential shear stress available on the road surface when it slides laterally. Thus the cyclic change in shear stress is

$$\tau_{max} = \mu \, P_{av}(x) \tag{31}$$

From ref. [1], the strain energy per unit tread volume is

$$U = \frac{(1+\mu)}{E} \, \tau_{max}^2$$

This gives the hysteretic loss per unit tread volume as

$$W_s = U.\tan\delta \tag{32}$$

This loss is assumed to be uniformly distributed throughout the tread elements lying on the surface.

Illustrations of the variation of the hysteretic loss due to cyclic shear stresses in eq. (32) and the scrubbing work in eq. (17) with yaw angle are shown in Figure 6 for a 40x14/22PR aircraft tire.

TEST PROGRAM

A test program was conducted to provide data on the temperature distribution in an aircraft tire during cornering operations. The results of these tests provided both insight into the general phenomena associated with a yawed rolling tire as well as a great deal of data which could be used to evaluate the validity of the analytical model described above.

A 40x14/22 PR aircraft tire was used in this test program. The tire was instrumented with an extensive set of thermocouples.

The installation of the thermocouples was begun by carefully laying out the desired locations on the surface of the tire. A typical set of such locations is illustrated in Figure 7. It can be seen in this figure that a thorough picture of the temperature distribution can be obtained with these locations, both through the thickness of the carcass as well as around the meridian of the cross-section.

Following the layout, small holes were drilled in the tire for implanting all interior thermocouples. The tires were then transferred to a commercial retreader where the tread was buffed off and the thermocouples in the tread region installed just prior to retreading. After the retreading process, the tires were returned to the laboratory where all remaining thermocouples were inserted in their proper locations and sealed with a hot patch process.

The test tire was tested on the automated 120-inch diameter dynamometer at the Air Force Flight Dynamics Laboratory, Wright-

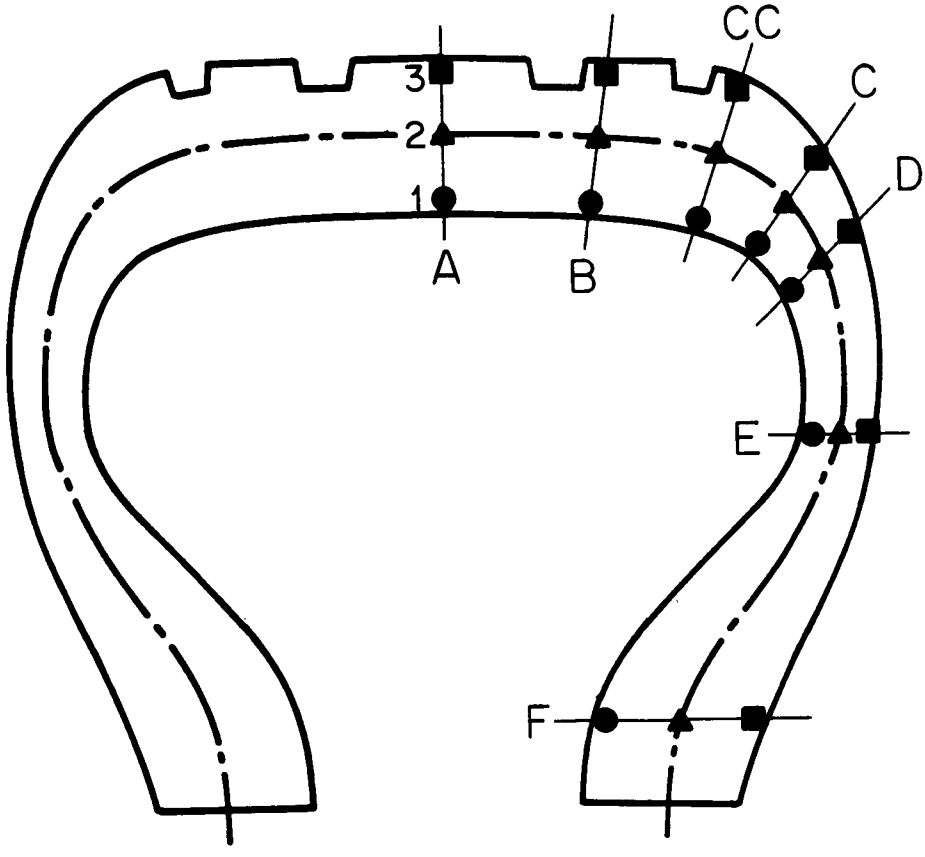

Fig. 7. Location of thermocouples in 40x14, 22 PR test tire used in yawed rolling thermal study.

Patterson Air Force Base. This dynamometer features a cantilevered wheel mounting fixture which is hydraulically loaded against the driven dynamometer wheel. The radial load on the tire is measured by strain gage beams in the mounting fixture. The thermocouple signals are collected through slip rings in an exterior data logger.

The tests were conducted under a variety of inflation pressures, vertical loads, vertical deflections, and yaw angles. These conditions are listed in Table 1.

Measured temperature profiles are shown in Figures 8-18. These are composite plots of all of the measured temperature values in the test program, as a function of time, for a speed of twenty miles per hour and at various operating conditions. The ordinate of these plots is the temperature rise above the initial temperature value and the abscissa is time. These figures consist of a set of plots, each of which represents one of the thermocouple locations noted in Figure 7. In general it is observed that the inside surface temperatures are highest outside of the contact region, while in the contact region the mid-line and outside temperatures are generally higher than the inside ones.

A careful examination of Figure 12 and 17, and 13 and 14 at location CC leads to another interesting observation, as well as providing some validity to the assumed nature of the contact geometry discussed above. From Figure 7 it can be seen that location CC is near the edge of contact for the deflections involved in these four tests. However, in Figures 12 and 13 the

Table 1

Operating Conditions - Yaw Tests 40x14, 22PR

Load lbs.	Deflection in.	Deflection %	Pressure psi	Yaw Angle deg.	Speed MPH
9900	1.97	49	140	0	20
14700	2.63	75	140	0	20
17850	2.66	76	175	0	20
17850	2.66	76	175	+1.5	20
17850	2.66	76	175	+3	20
14700	2.63	75	140	+3	20
14700	2.63	75	140	-3	20
9900	1.97	49	140	+3	20
9900	1.97	49	140	-3	20
17850	2.66	76	175	-3	20
25000	4.51	130	118	0	20

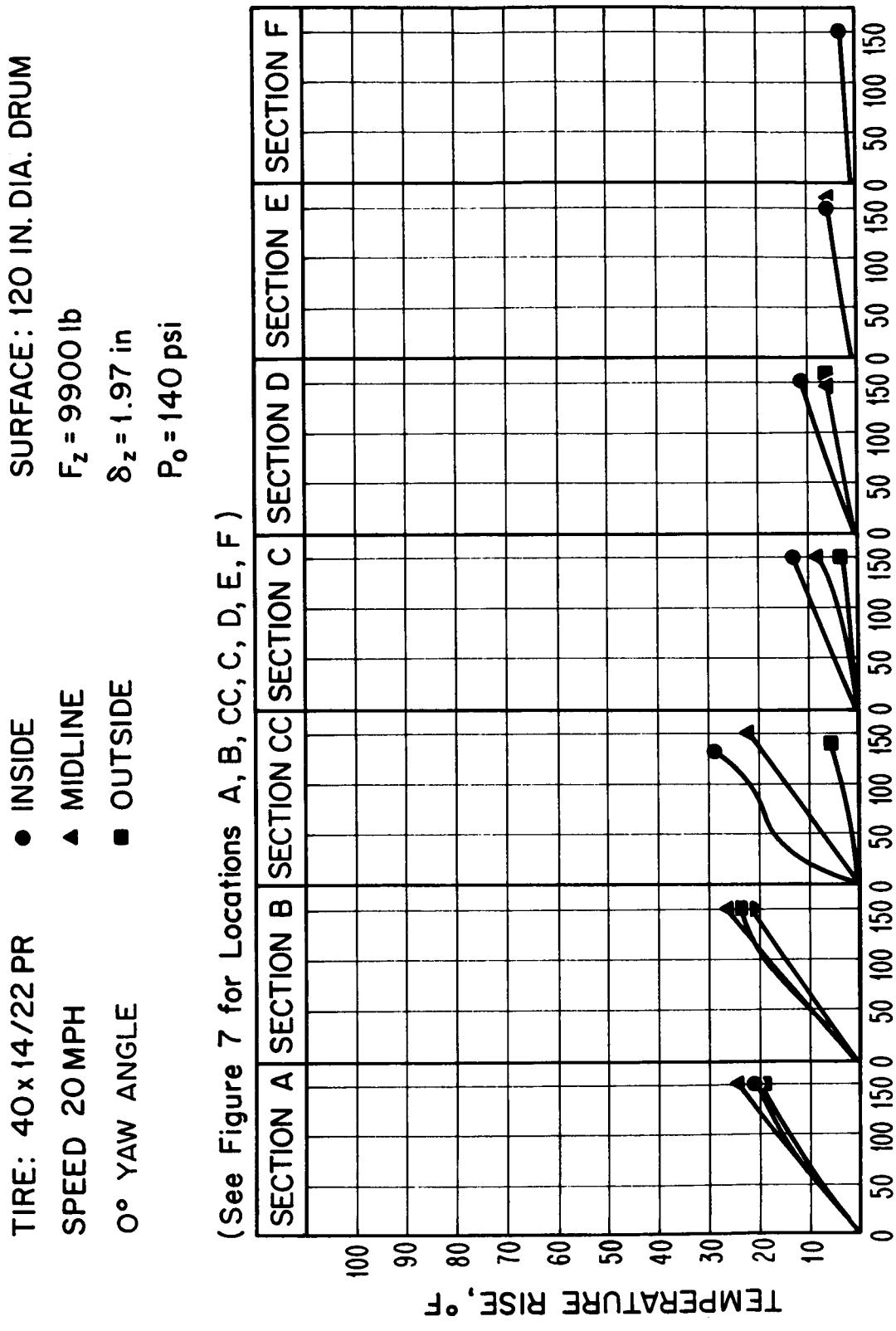

Fig. 8. Experimental temperature profile data vs time.

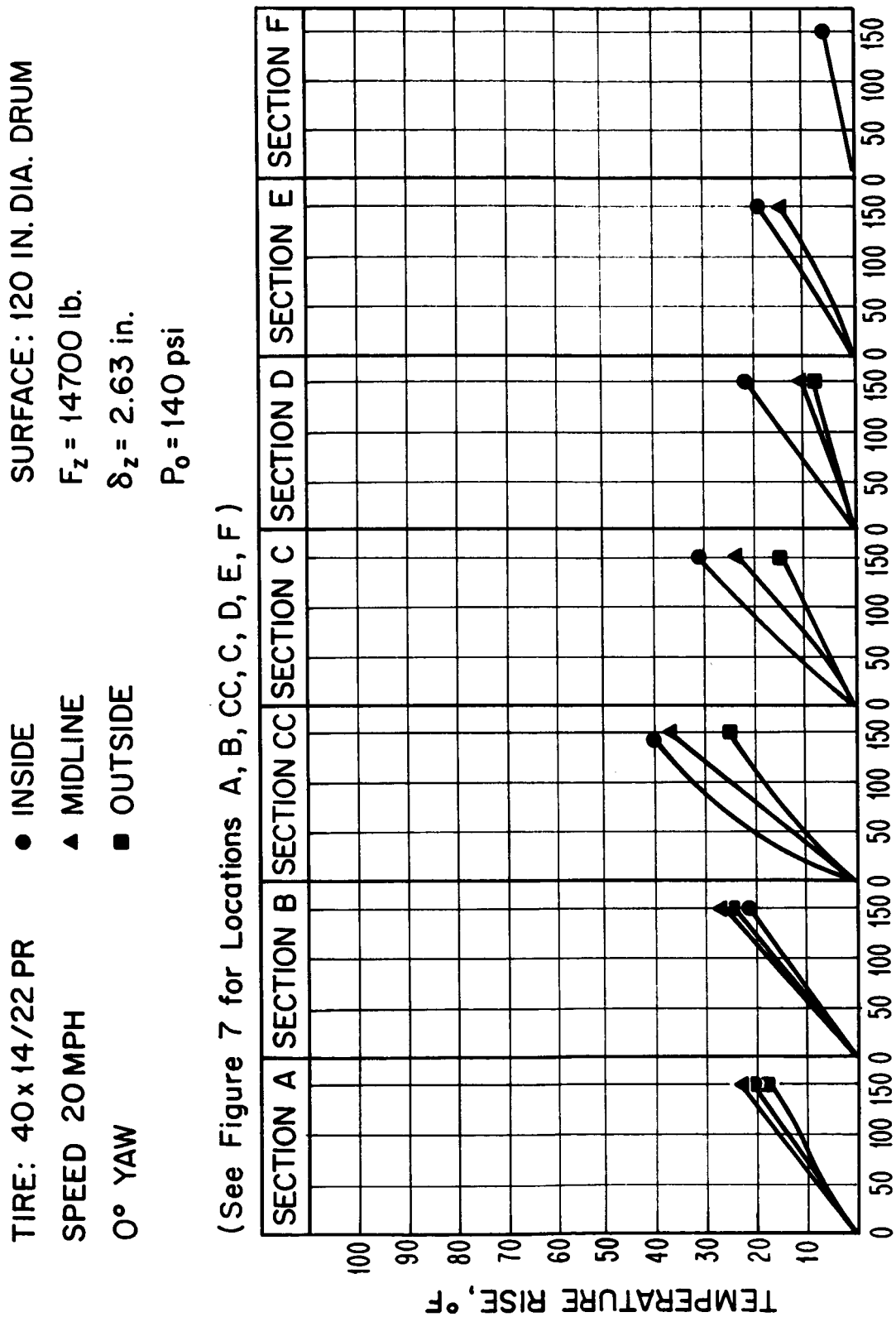

Fig. 9. Experimental temperature profile data vs time.

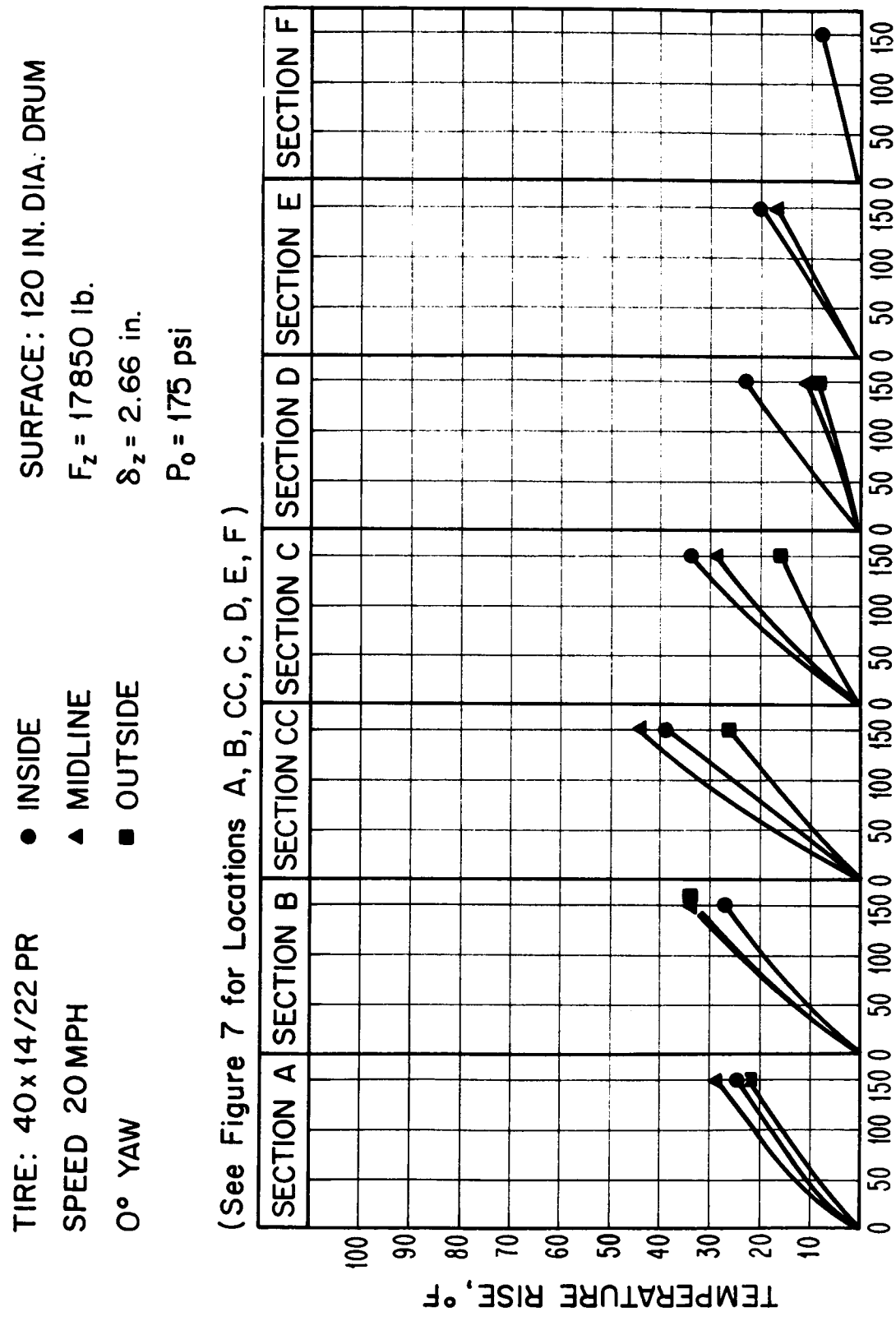

Fig. 10. Experimental temperature profile data vs time.

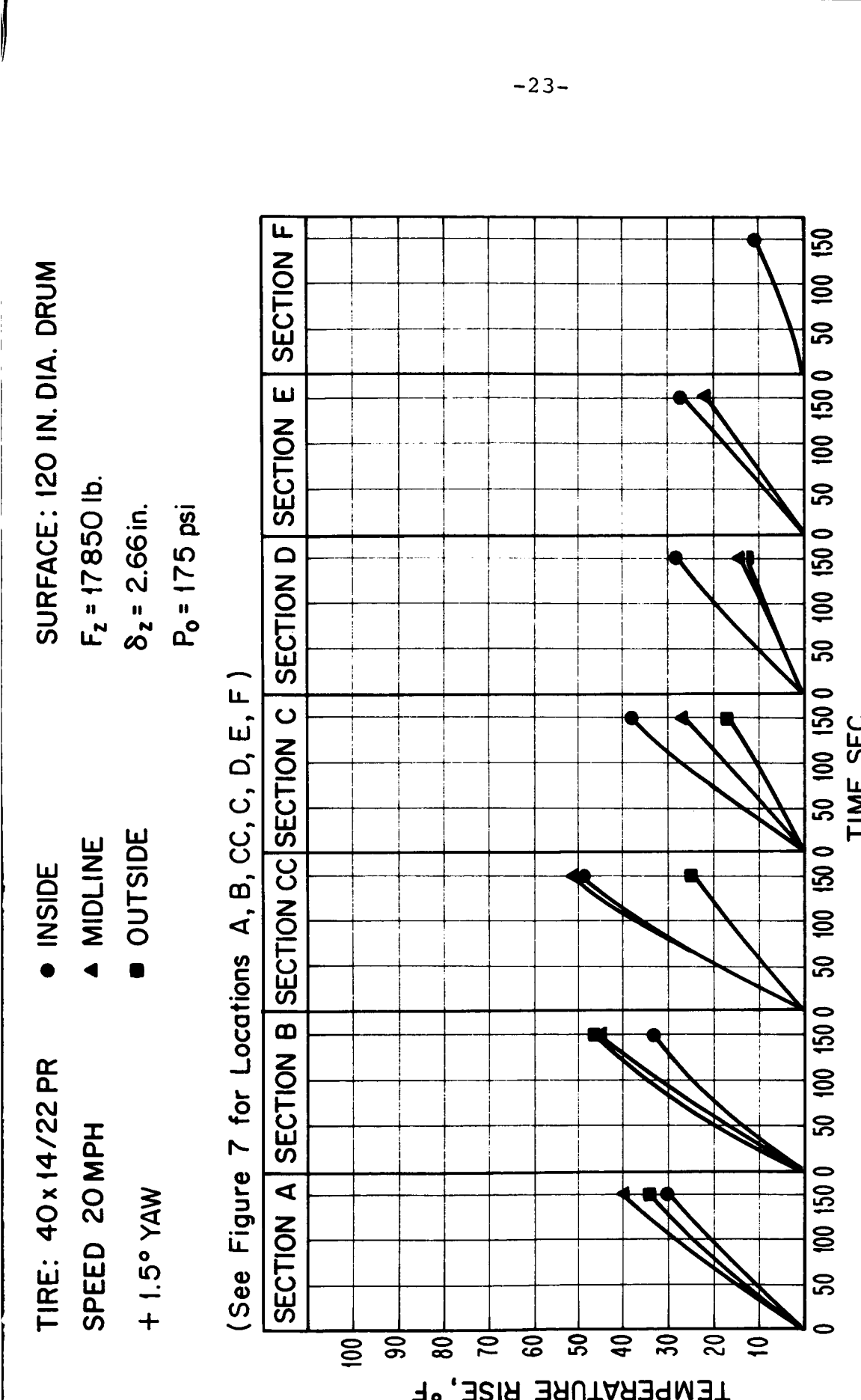

Fig. 11. Experimental temperature profile data vs time

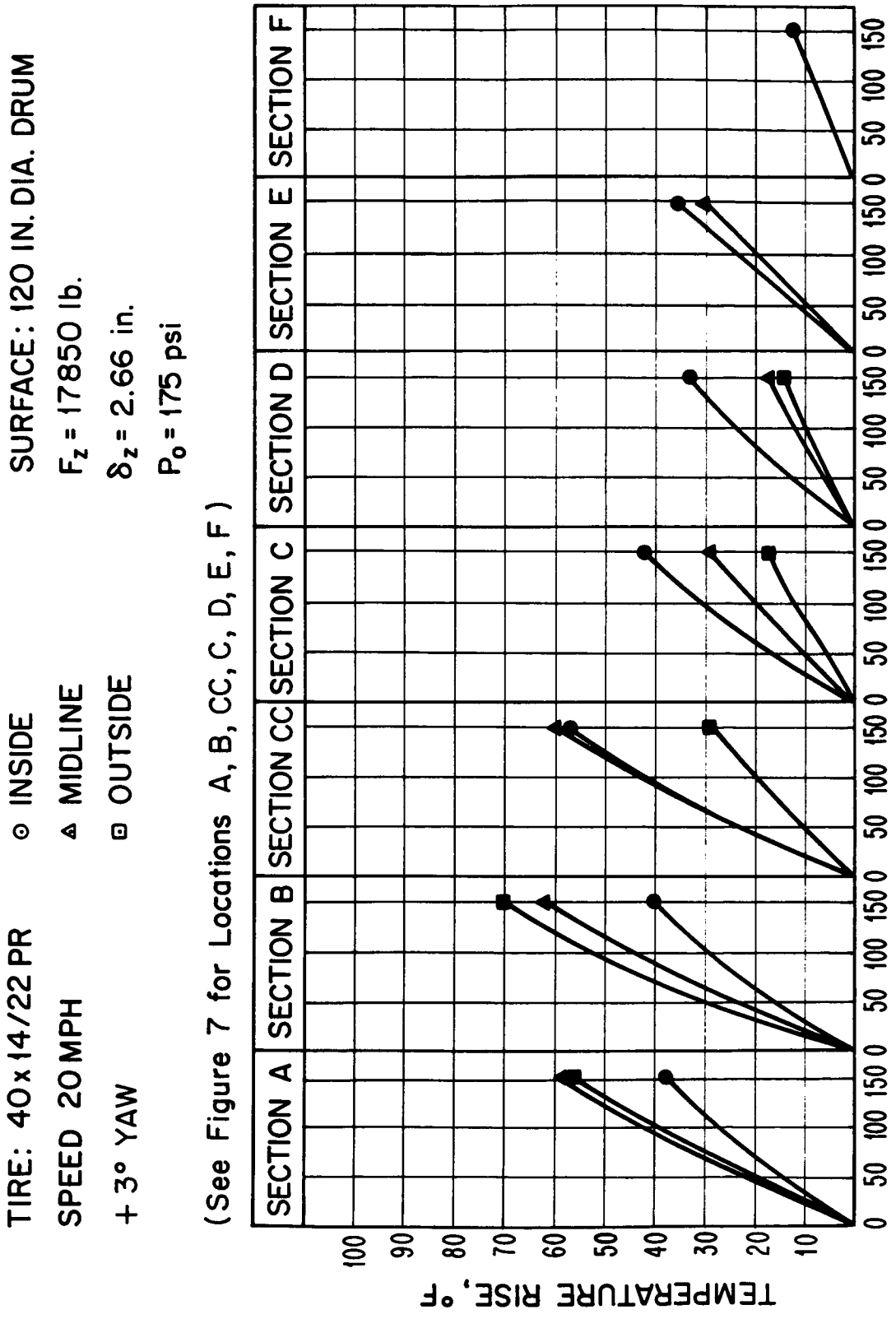

Fig. 12. Experimental temperature profile data vs time.

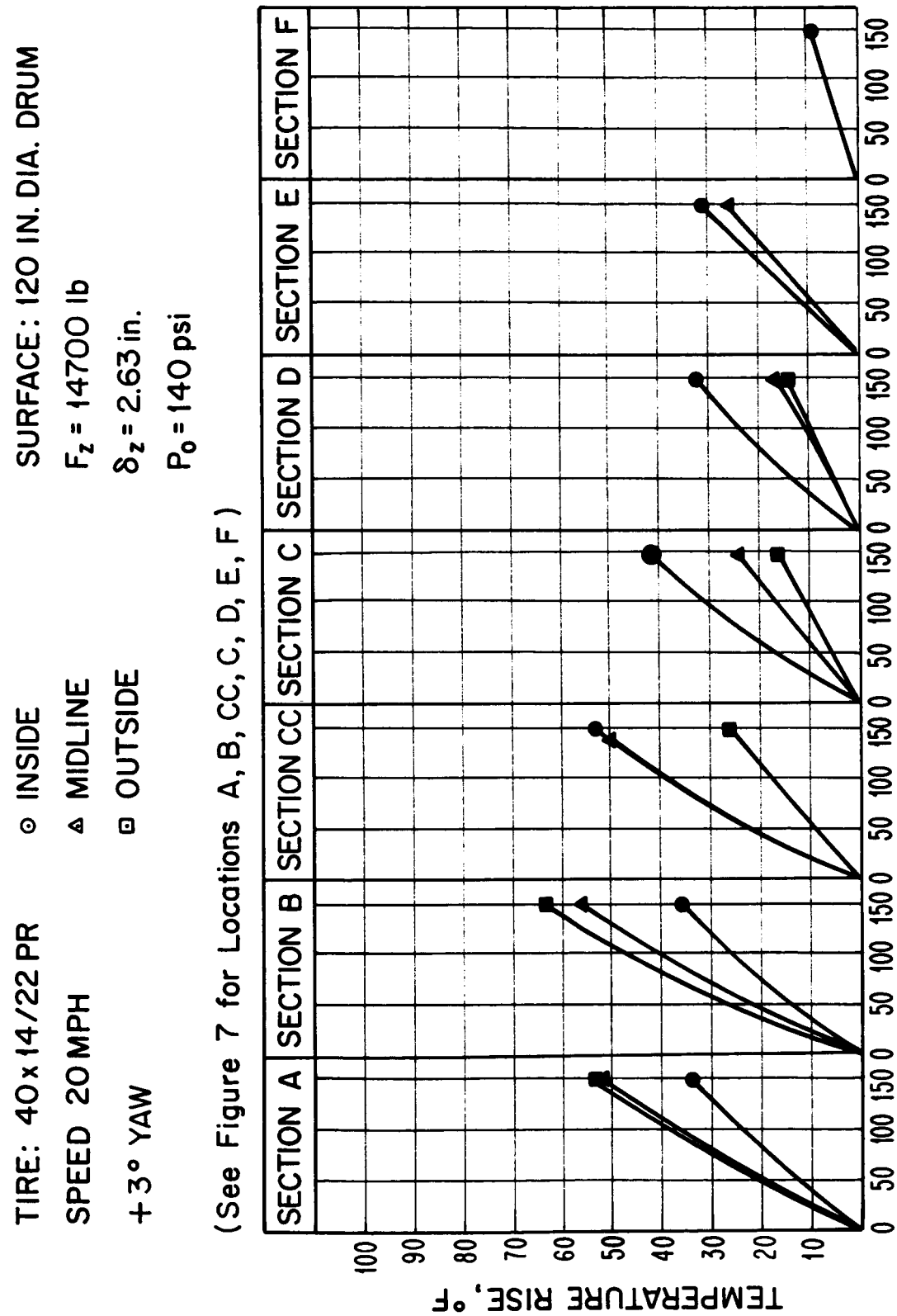

Fig. 13. Experimental temperature profile data vs time.

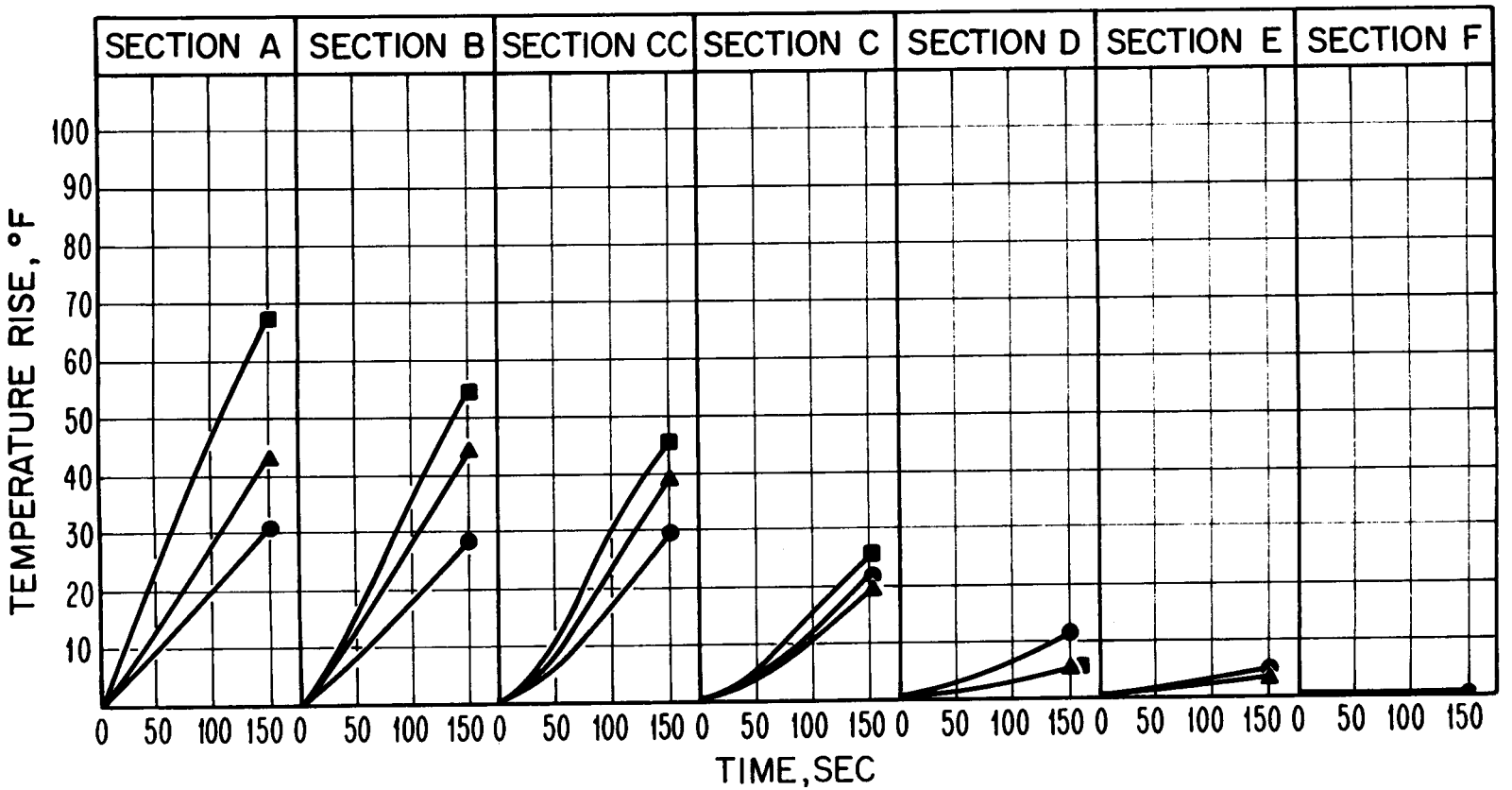

Fig. 14. Experimental temperature profile data vs time.

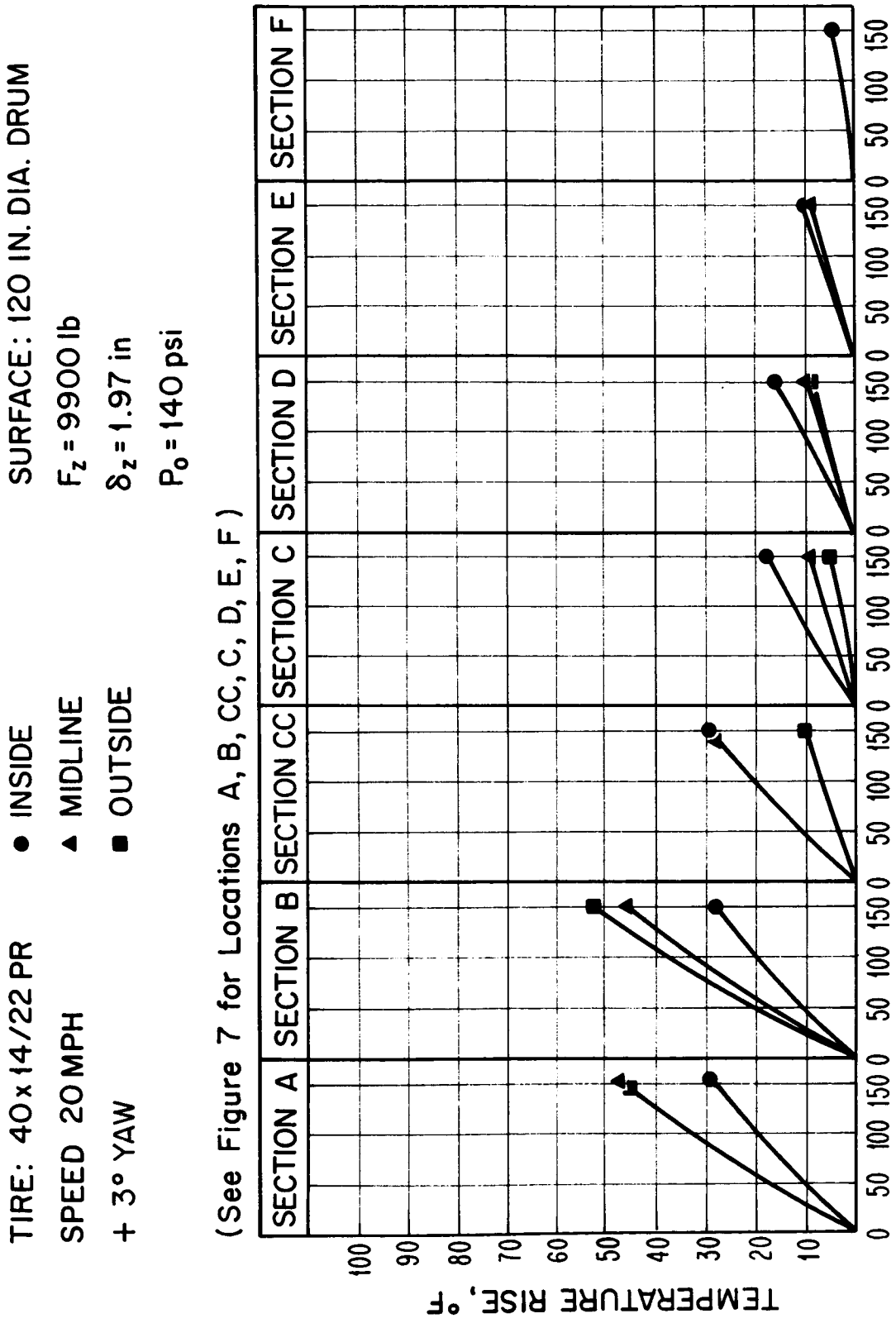

Fig. 15. Experimental temperature profile data vs time.

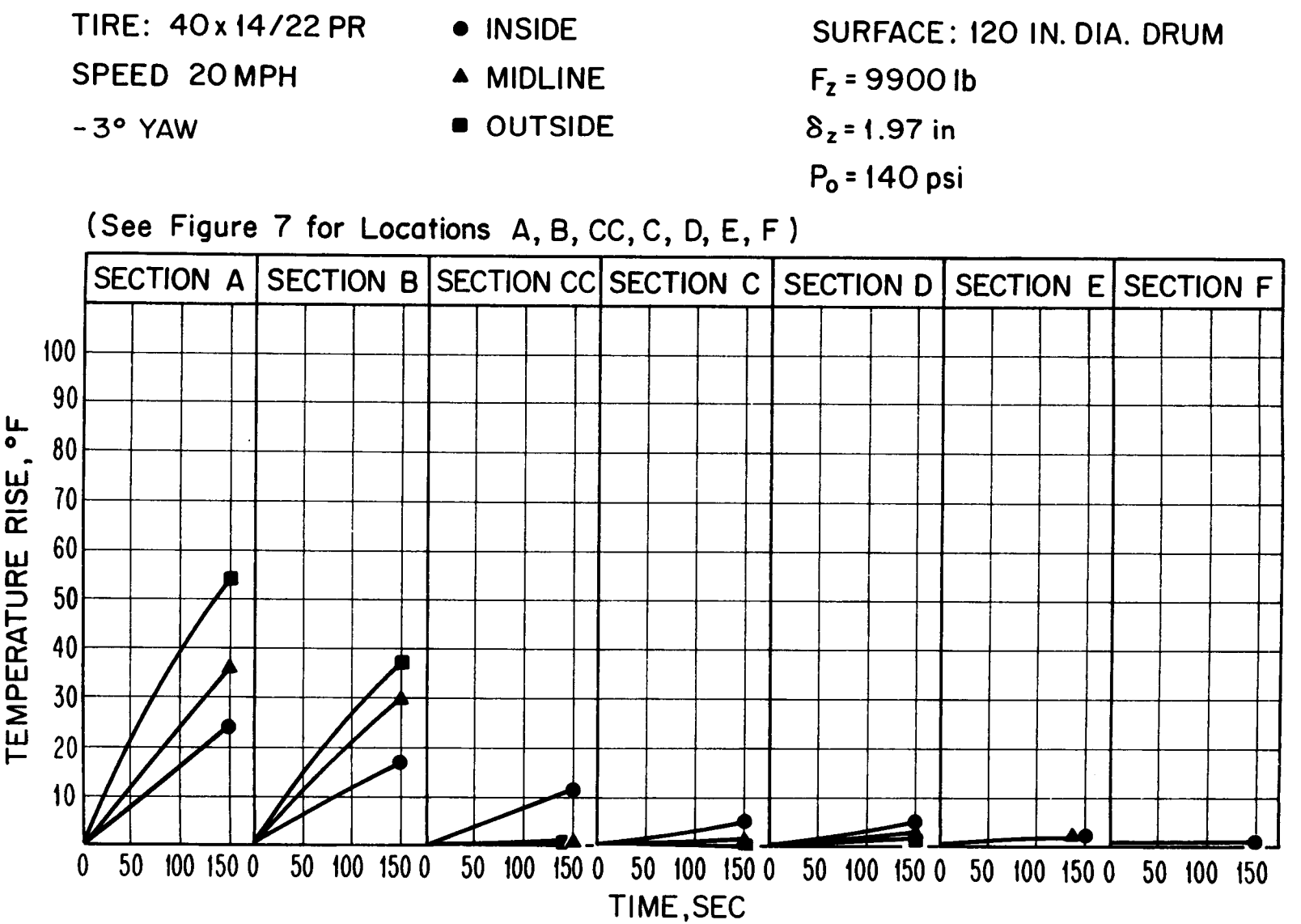

Fig. 16. Experimental temperature profile data vs time.

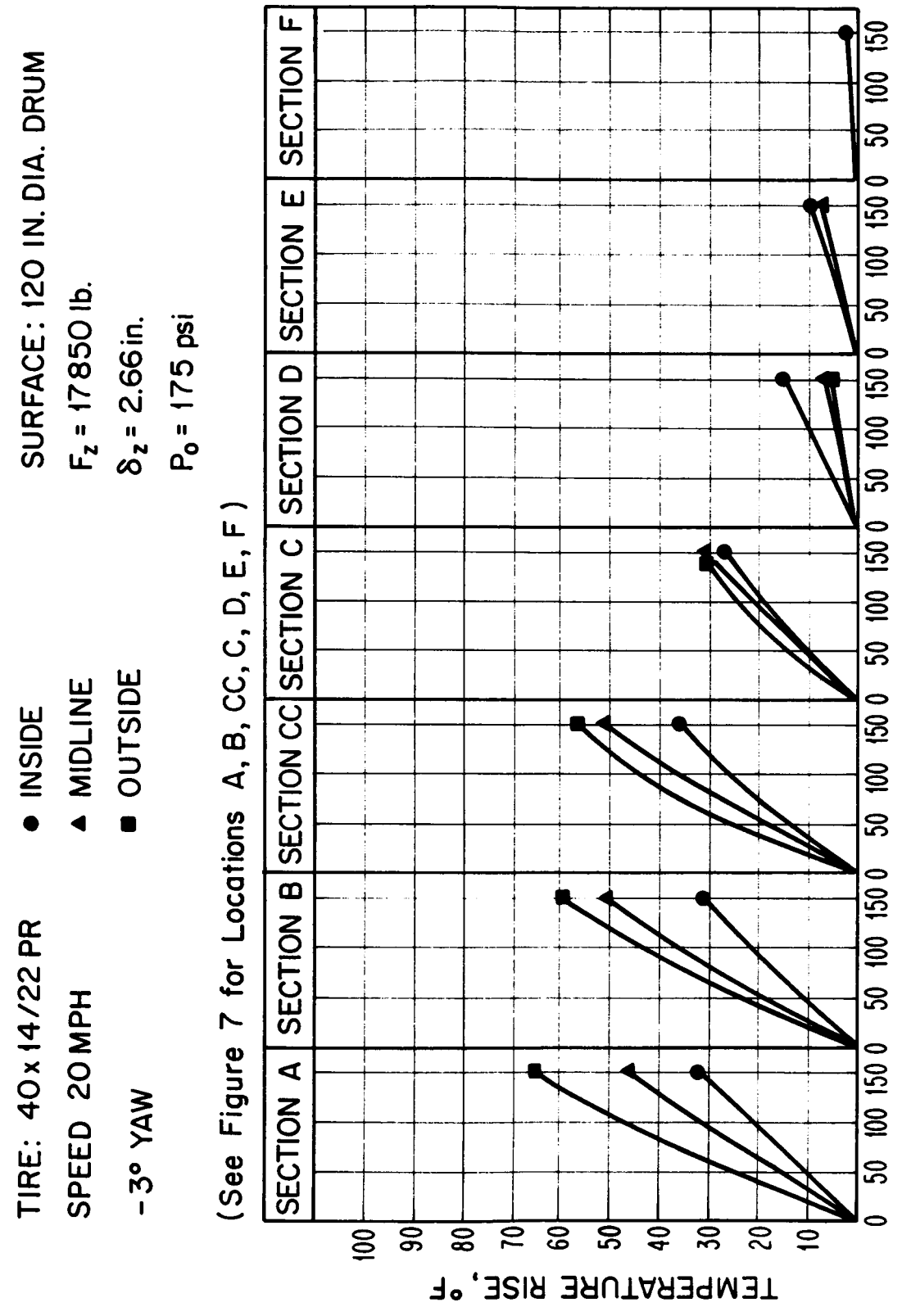

Fig. 17. Experimental temperature profile data vs time.

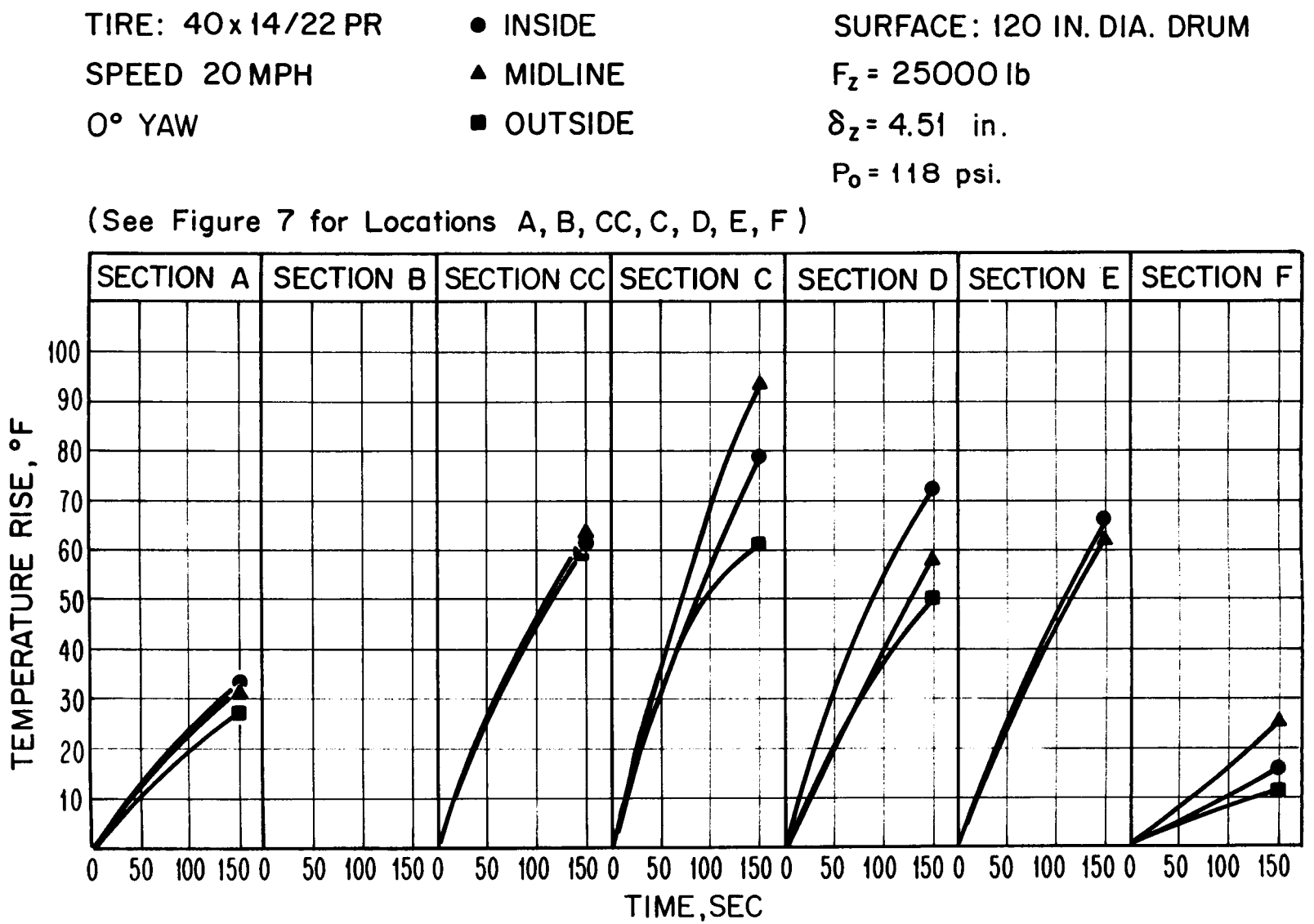

Fig. 18. Experimental temperature profile data vs time.

temperature distribution resembles that which takes place in those regions out of contact, especially towards the inside surface. This is a clear indication that the outboard shoulder is being deformed out of contact during yawed rolling. On the other hand, from Figures 14 and 17 it is noted that the temperature distribution in location CC is very similar in nature to that which occurs in the contact region. This is an indication that during yawed rolling the inboard shoulder is being deformed into the contact region. The results in Figure 15 and 16, which also plot measurements from the inboard and outboard sides for the same operating conditions, indicate that location CC is out of contact. This was indeed the case, since the vertical deflection was smaller for these tests.

The next set of Figures, 19-26, present test data at a fixed time to show the effect of four operating parameters, namely tire deflection, tire inflation pressure, yaw angle, and direction of cornering.

The effect of deflection on temperature distribution in the tire carcass for both the outboard and inboard sides is illustrated in Figures 19 and 20. The ordinate in these plots again represent the temperature rise above the initial temperature. The abscissa represents the meridianal location of the thermocouples. All of the data represents the measured temperature rise after 150 seconds at 20 miles per hour. As expected, the highest temperatures occur with the higher deflections, both on the inboard and outboard sides of the tire. The differences in temperature rise for the two deflections appear larger on the inside and mid-line than they do near the outside surface.

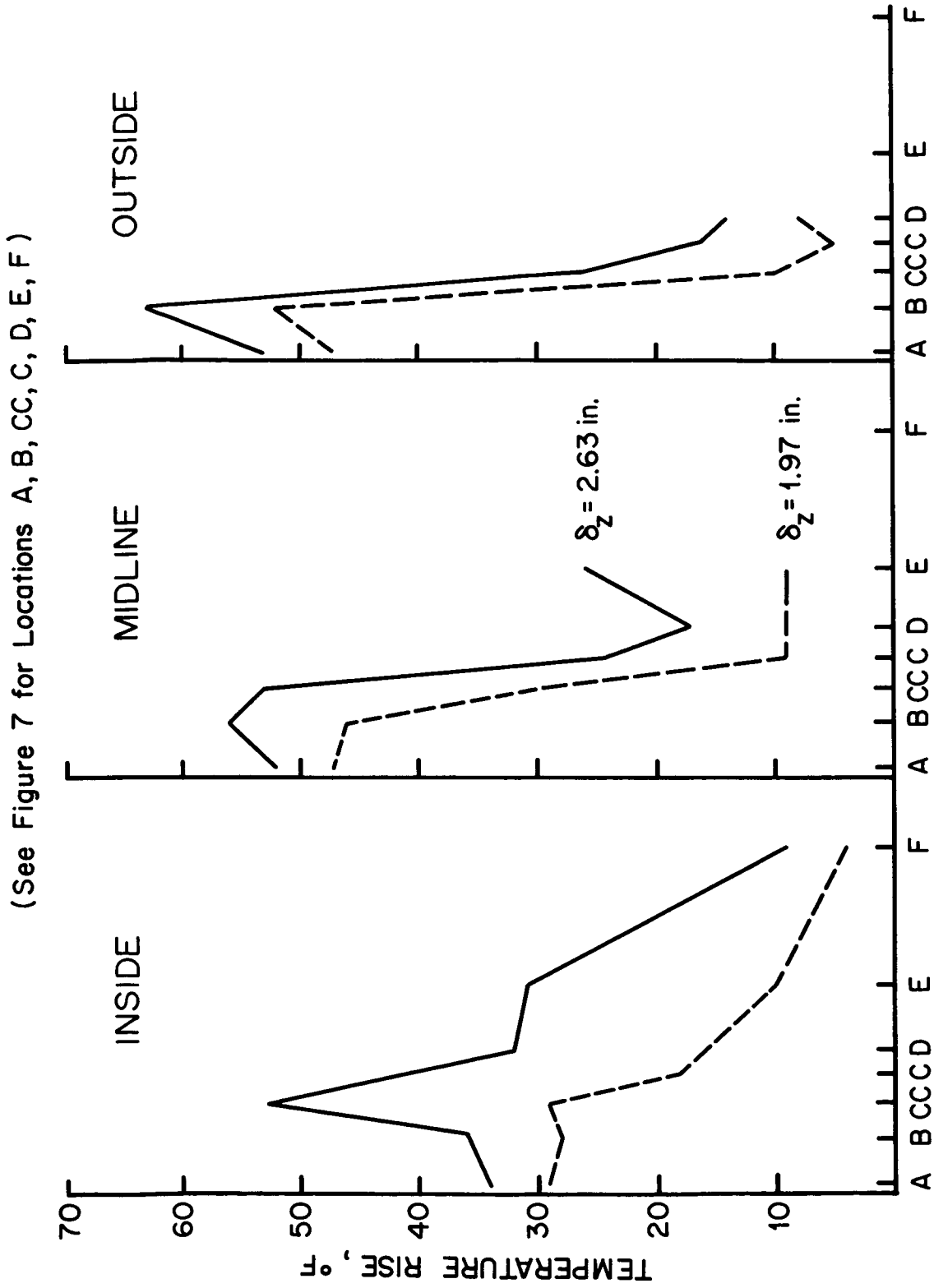

Fig. 19. Effect of deflection on temperature distribution in 40x14/22 PR tire, inflation pressure = 140 psi, yaw angle = +3°, t = 150 sec. at 20 MPH.

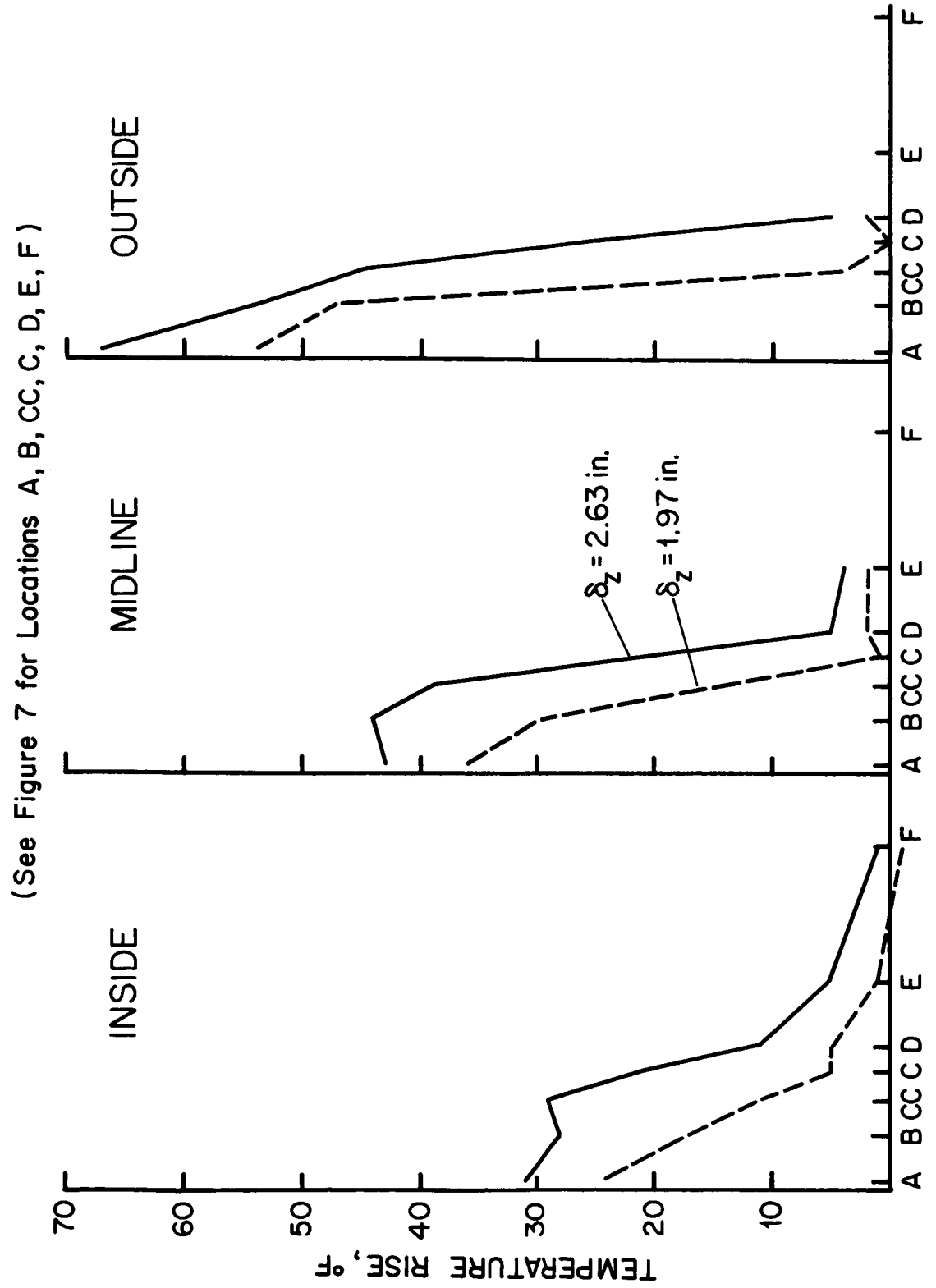

Fig. 20. Effect of deflection on temperature distribution in 40x14/22 PR tire, inflation pressure = 140 psi, yaw angle = -3^{o}, t = 150 sec. at 20 MPH.

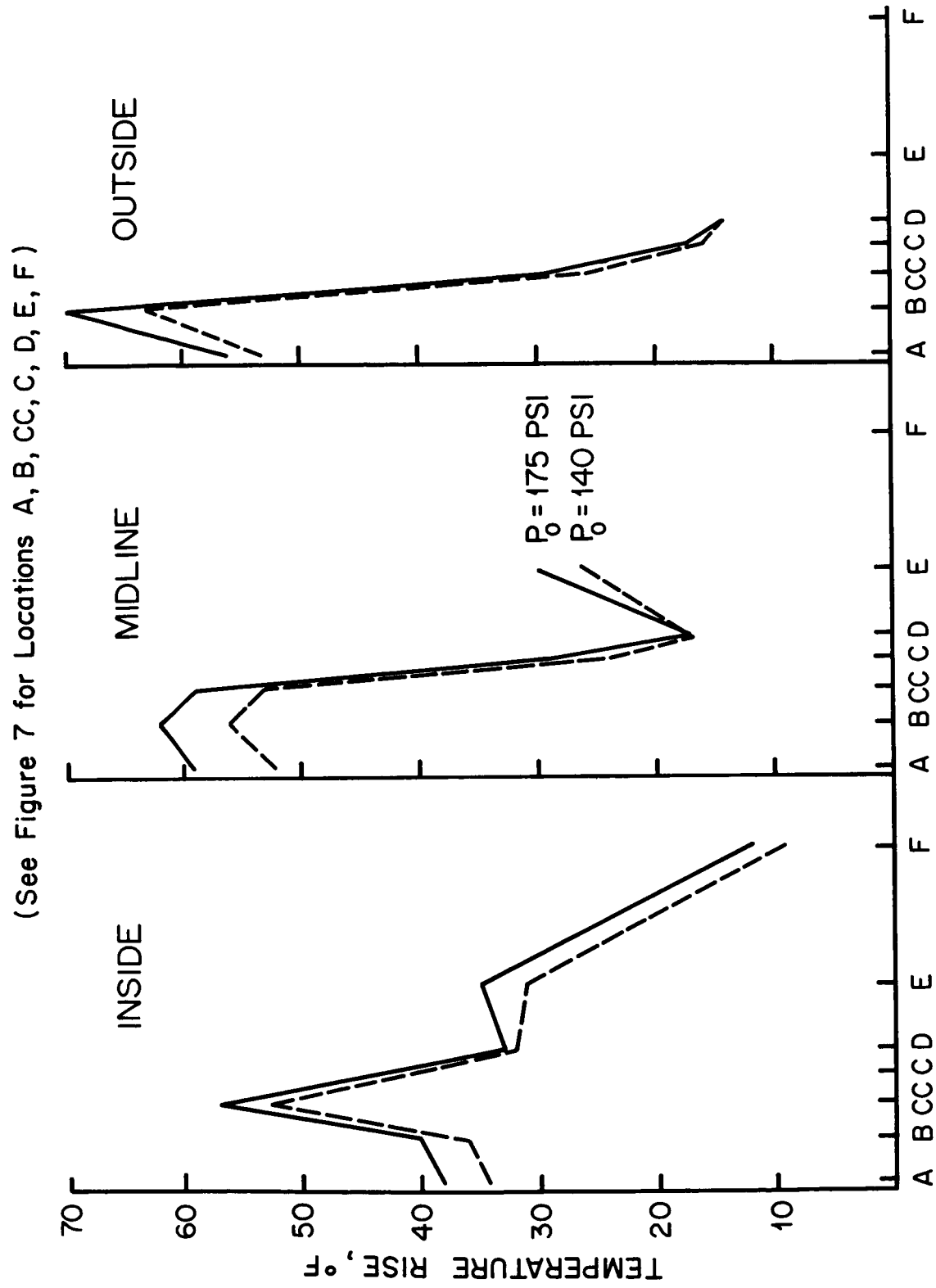

Fig. 21. Effect of initial inflation pressure on temperature distribution in 40x14/22 PR tire, vertical deflection $\simeq$ 2.65 in., yaw angle = +3°, t = 150 sec. at 20 MPH.

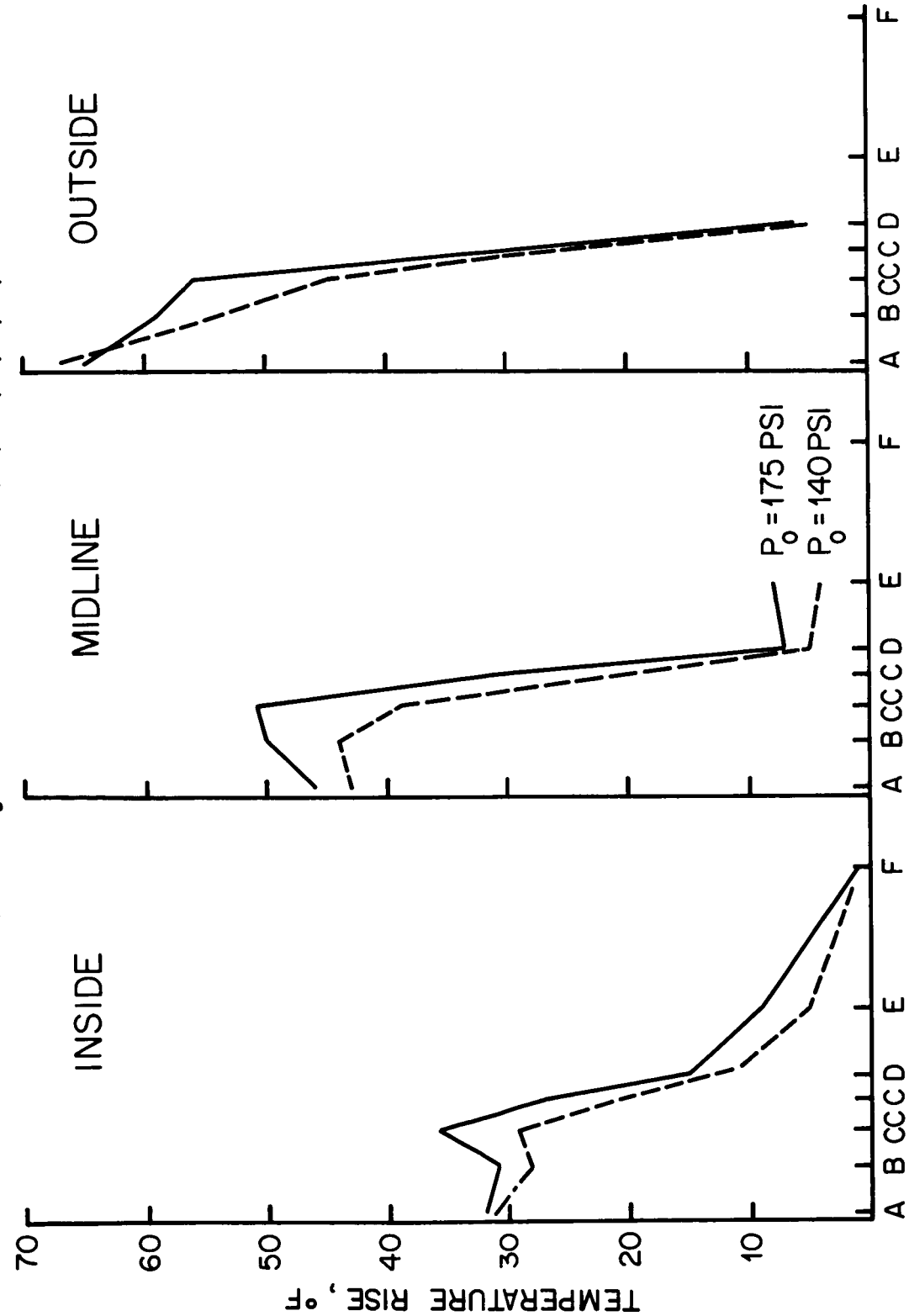

Fig. 22. Effect of initial inflation pressure on temperature distribution in 40x14/22 PR tire, vertical deflection ≃ 2.65 in., yaw angle = -3°, t = 150 sec. at 20 MPH.

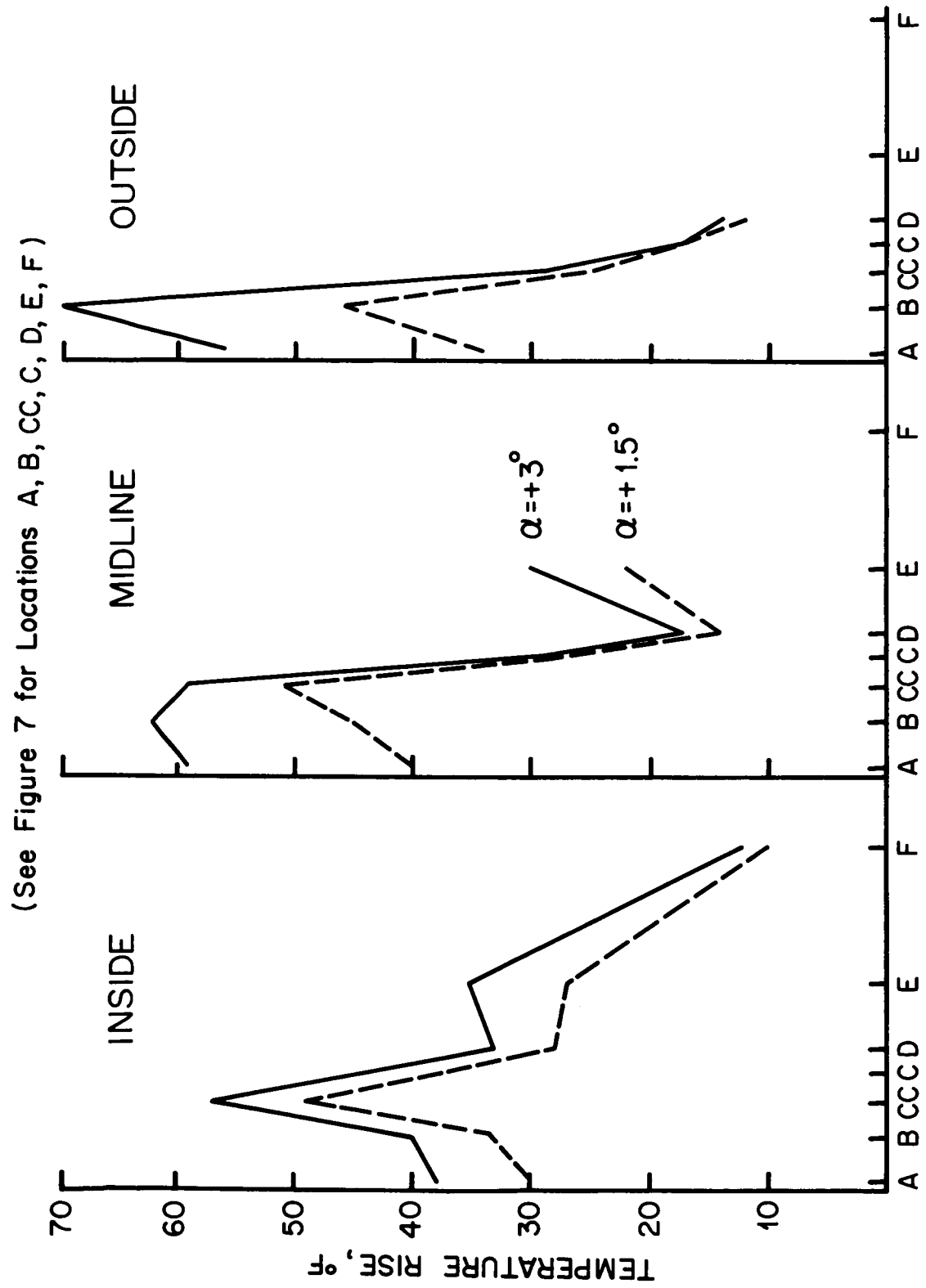

Fig. 23. Effect of yaw angle on temperature distribution in 40x14/22 PR tire, vertical deflection = 2.66 in., initial inflation pressure = 175 psi, t = 150 sec. at 20 MPH.

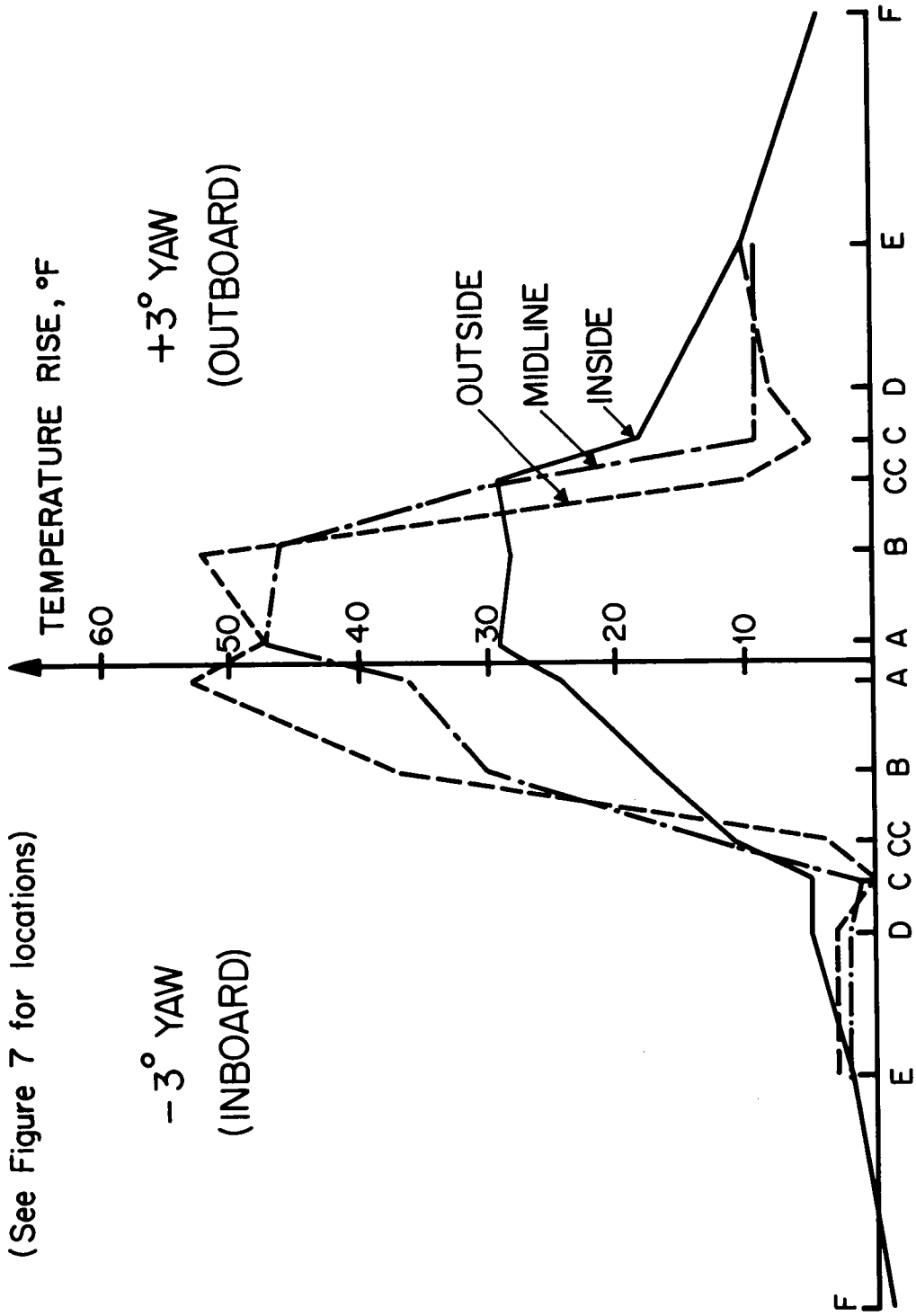

Fig. 24. Effect of direction of cornering on temperature distribution in 40x14/22 PR tire, vertical deflection = 1.97 in., inflation pressure = 140 psi, t = 150 sec. at 20 MPH.

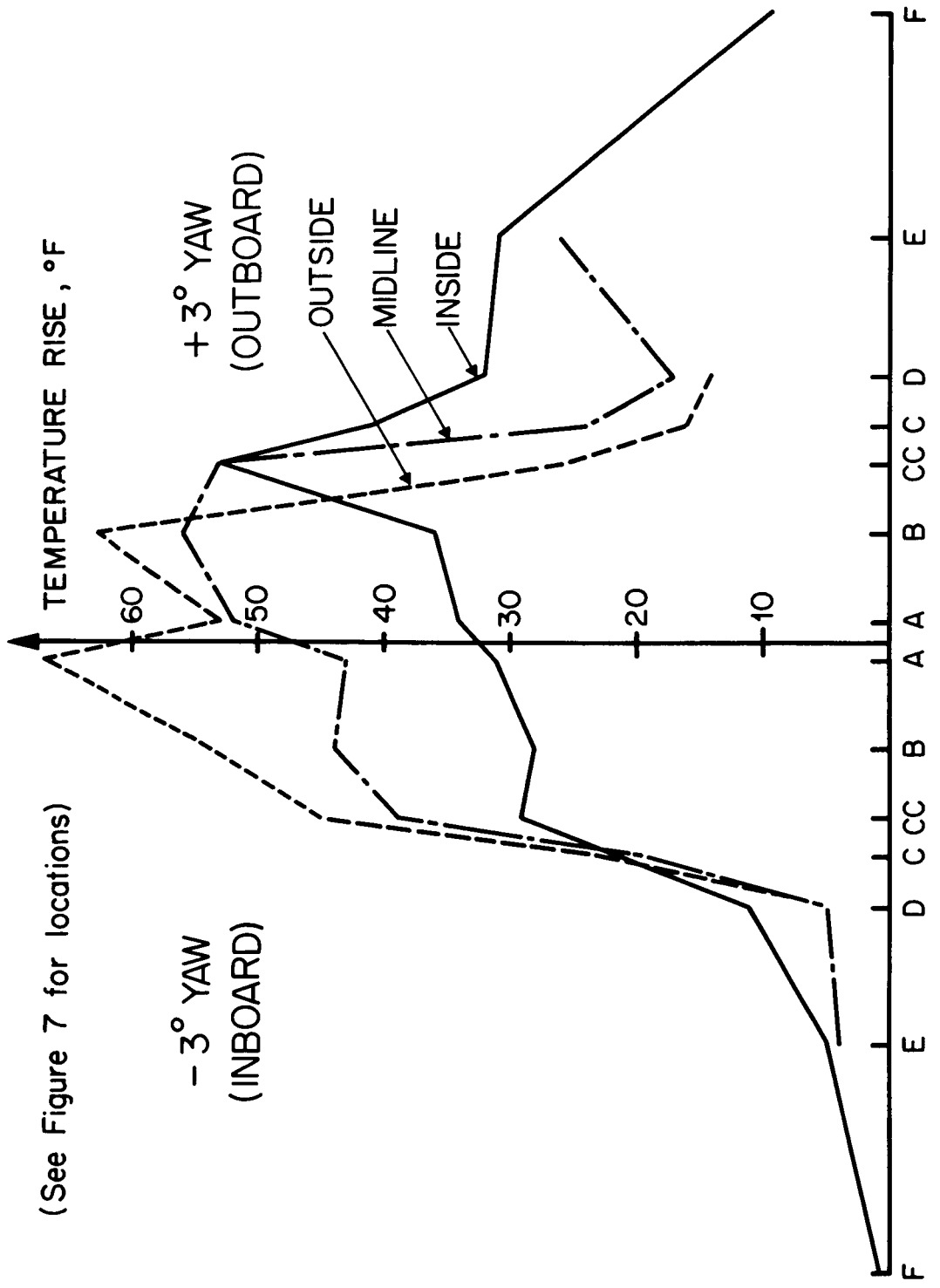

Fig. 25. Effect of direction of cornering on temperature distribution in 40x14/22 PR tire, vertical deflection = 2.63 in., inflation pressure = 140 psi, t = 150 sec. at 20 MPH.

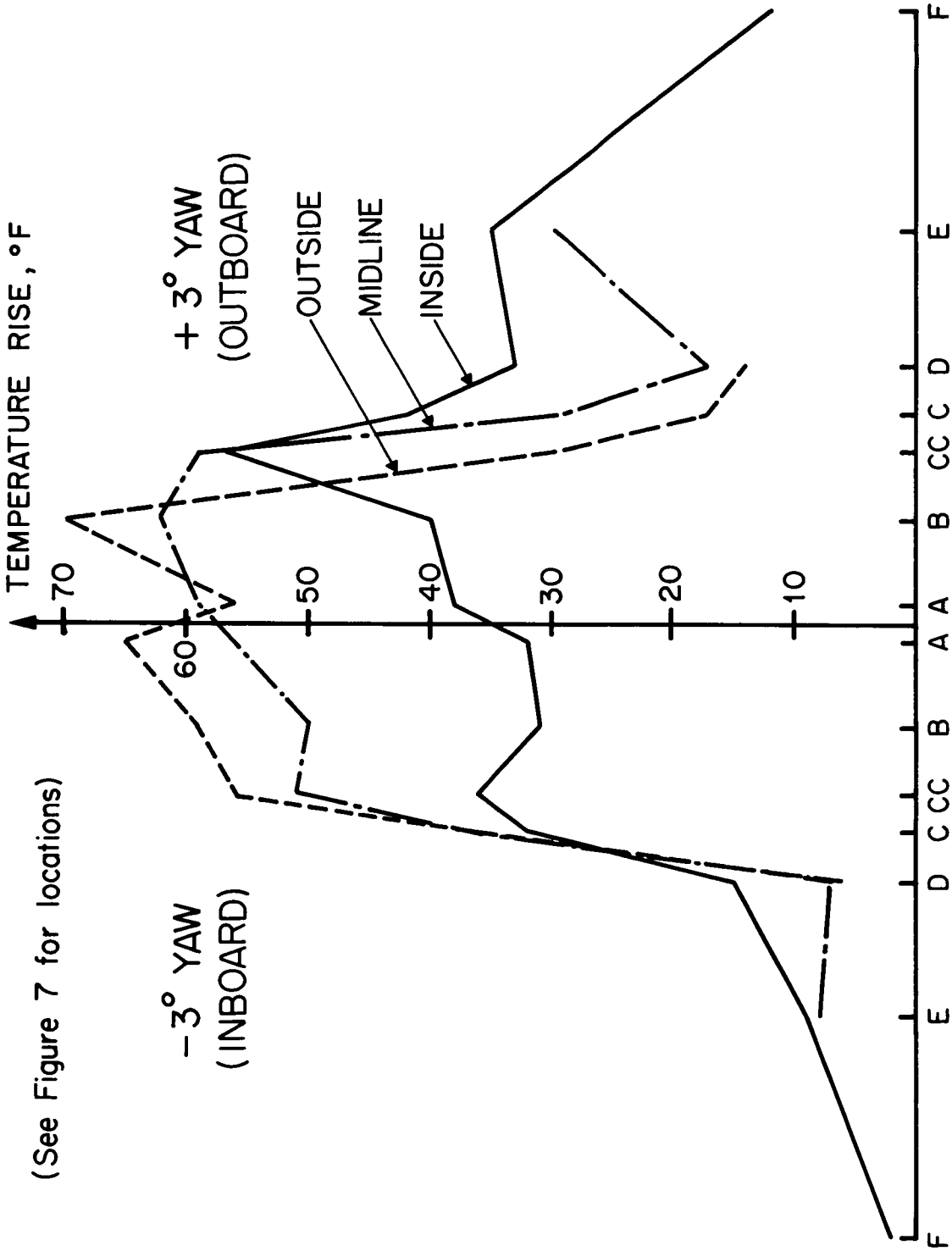

Fig. 26. Effect of direction of cornering on temperature distribution in 40x14/22 PR tire, vertical deflection = 2.66 in.,initial inflation pressure = 175 psi, t = 150 sec. at 20 MPH.

The effect of pressure on temperature distribution in the tire carcass for both the outboard and inboard sides is illustrated in Figures 21 and 22. Again these plots are temperature rise after 150 seconds at 20 miles per hour. As can be seen, the temperature distribution is not affected appreciably by the different initial inflation pressures reported here.

The effect of yaw angle on temperature distribution in the tire carcass is illustrated in Figure 23. Again these plots are temperature rise around the meridian after 150 seconds at 20 miles per hour. As expected, the temperature rise is largest for larger yaw angles. However, this is much more pronounced in the contact region than it is out of contact. This is especially true of those elements from the mid-surface to the outside surface of the tread.

The difference in temperature distribution for the inboard and outboard sides of the tire is illustrated in Figures 24-26. As expected, the distributions are not symmetrical about the center of contact. Also it is clear that the nature of the distribution varies through the thickness as well as around the meridian. However, in general, except for the outside elements in the contact region, the inboard temperature rises are less than the corresponding outboard ones.

COMPARISON OF ANALYSIS WITH EXPERIMENT

With the above experimental data available comparisons can be made between the calculation of temperature distributions in the tire and measured data. In order to carry out the computations appropriate material characteristics and geometries must be assigned to the tire. These data were provided from actual measurements as well as from various literature sources, as outlined in ref. [1].

Using a time increment of t=10 seconds, and using the appropriate material properties and geometries, computations were carried out for the temperature in the tire under operating conditions listed in Table 1. Some typical comparisons between calculations and experiment are shown in Figures 27-35.

Many comparisons were made of complete temperature profiles, as illustrated in Figure 27, where all of the meridianal and thickness locations are compared simultaneously for one of the test conditions listed in Table 1. As can be seen, the comparisons are reasonably good. This is only one typical time-temperature profile plot of the eleven possible such plots that could be generated from the test data illustrated in Figures 8-18. However, each of the other ten plots showed similar patterns so that the major trends of temperature rise for yawed rolling can be calculated adequately for short term taxi-takeoff conditions with the analytical model presented here.

To conclude the comparison of analysis with experiment four additional sets of plots are presented in Figures 28-35. These plots serve two purposes. First they illustrate typical

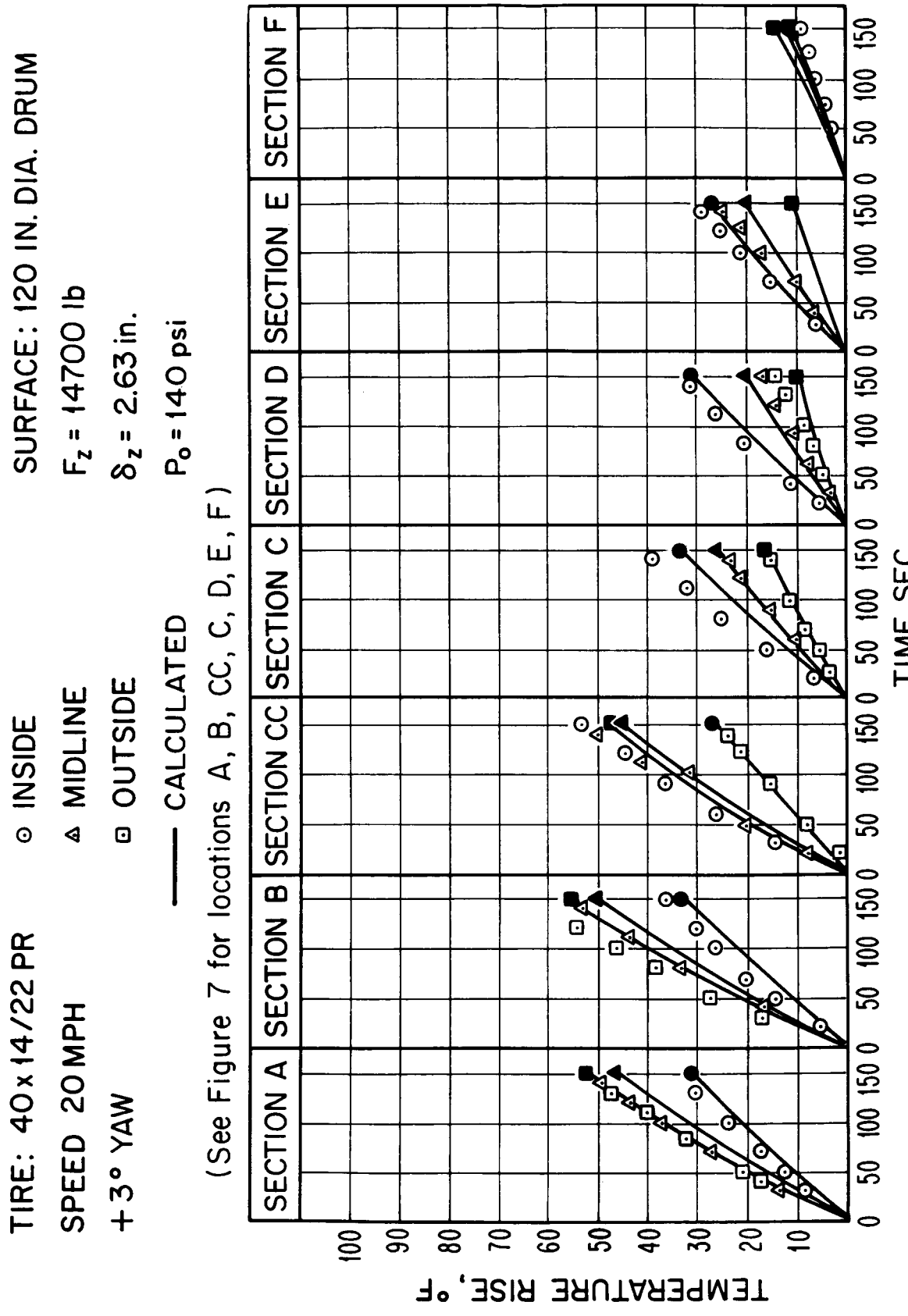

Fig. 27. Typical measured and calculated tire temperature profiles.

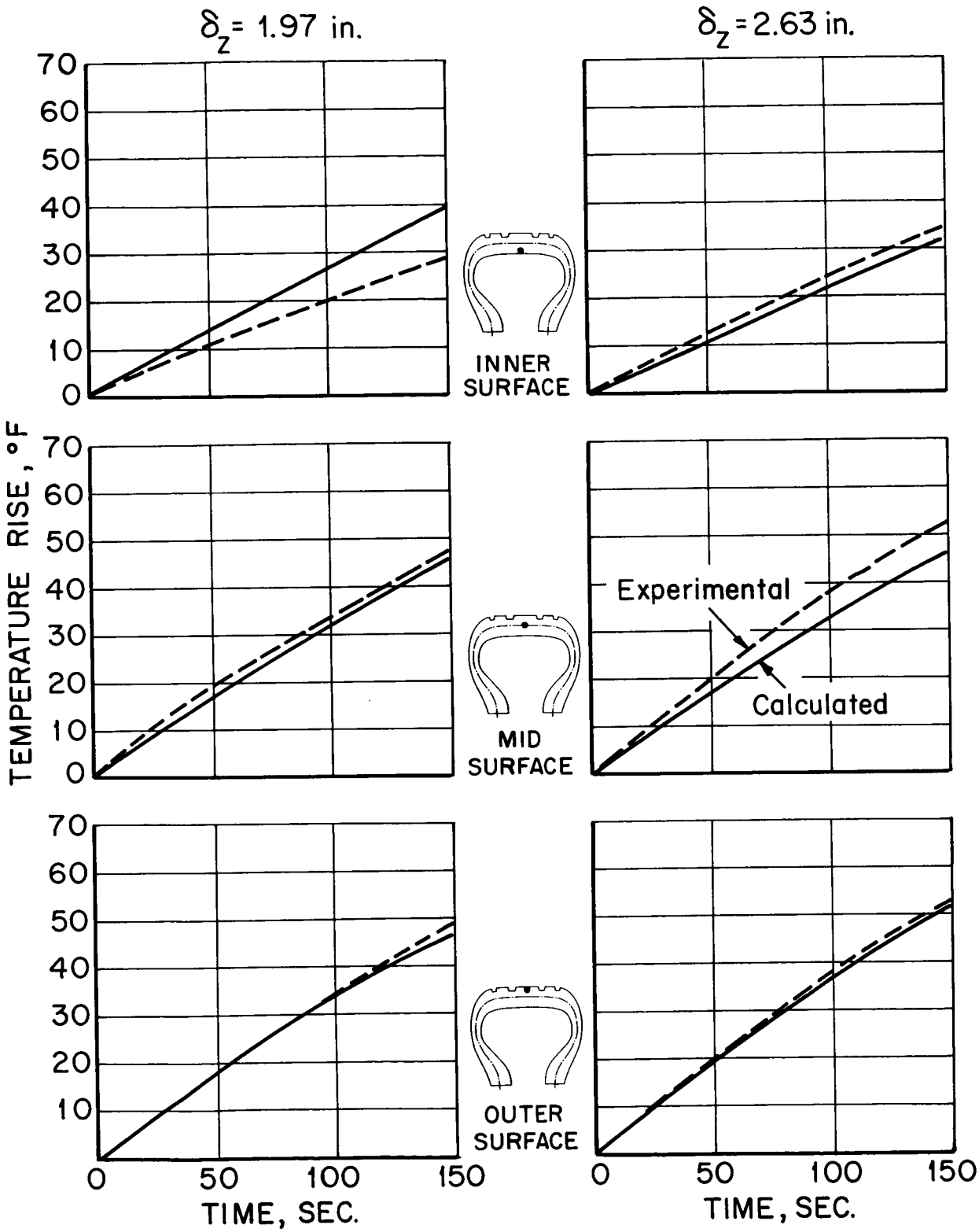

Fig. 28. Comparison of experimental and calculated temperature in the contact region for yawed rolling for two different deflections. 40x14/22 PR, P_o = 140 psi, $\alpha = +3^o$, V = 20 MPH.

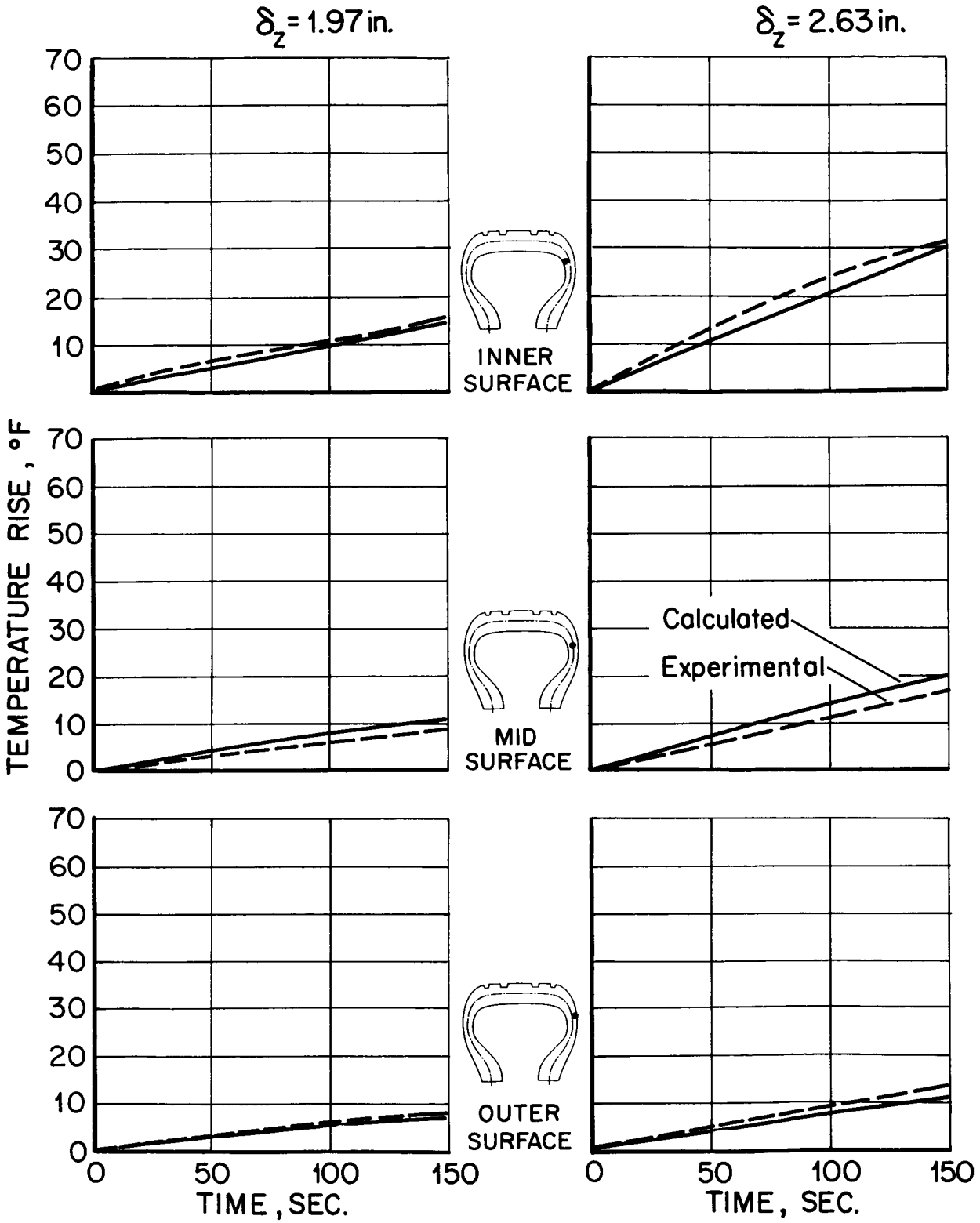

Fig. 29. Comparison of experimental and calculated temperature in upper sidewall region for yawed rolling for two different deflections. 40x14/22 PR, P_o = 140 psi, $\alpha = +3^o$, V = 20 MPH.

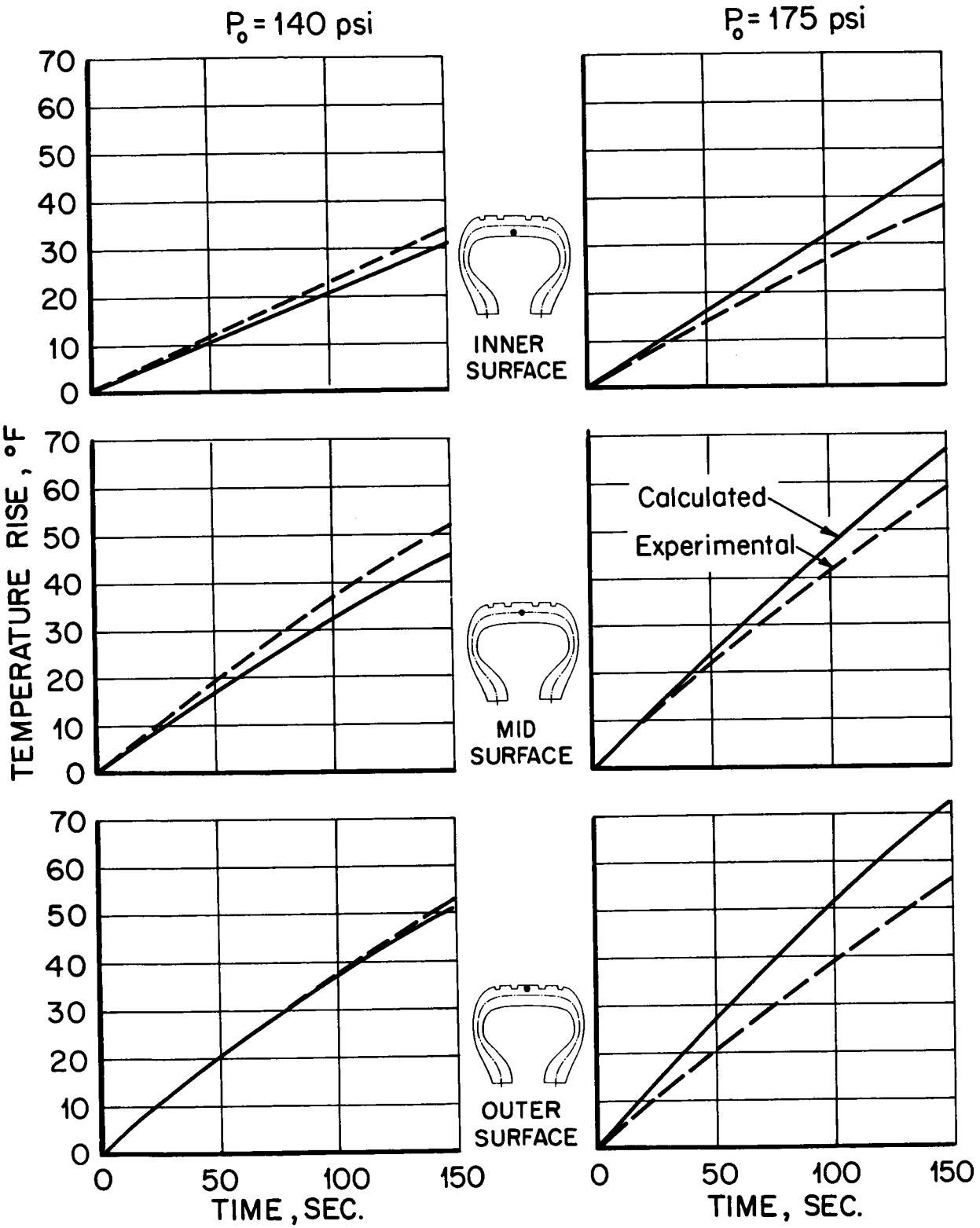

Fig. 30. Comparison of experimental and calculated temperature in contact region for yawed rolling for two different pressures. 40x14/22 PR, δ_z = 2.66, α = +3°, V = 20 MPH.

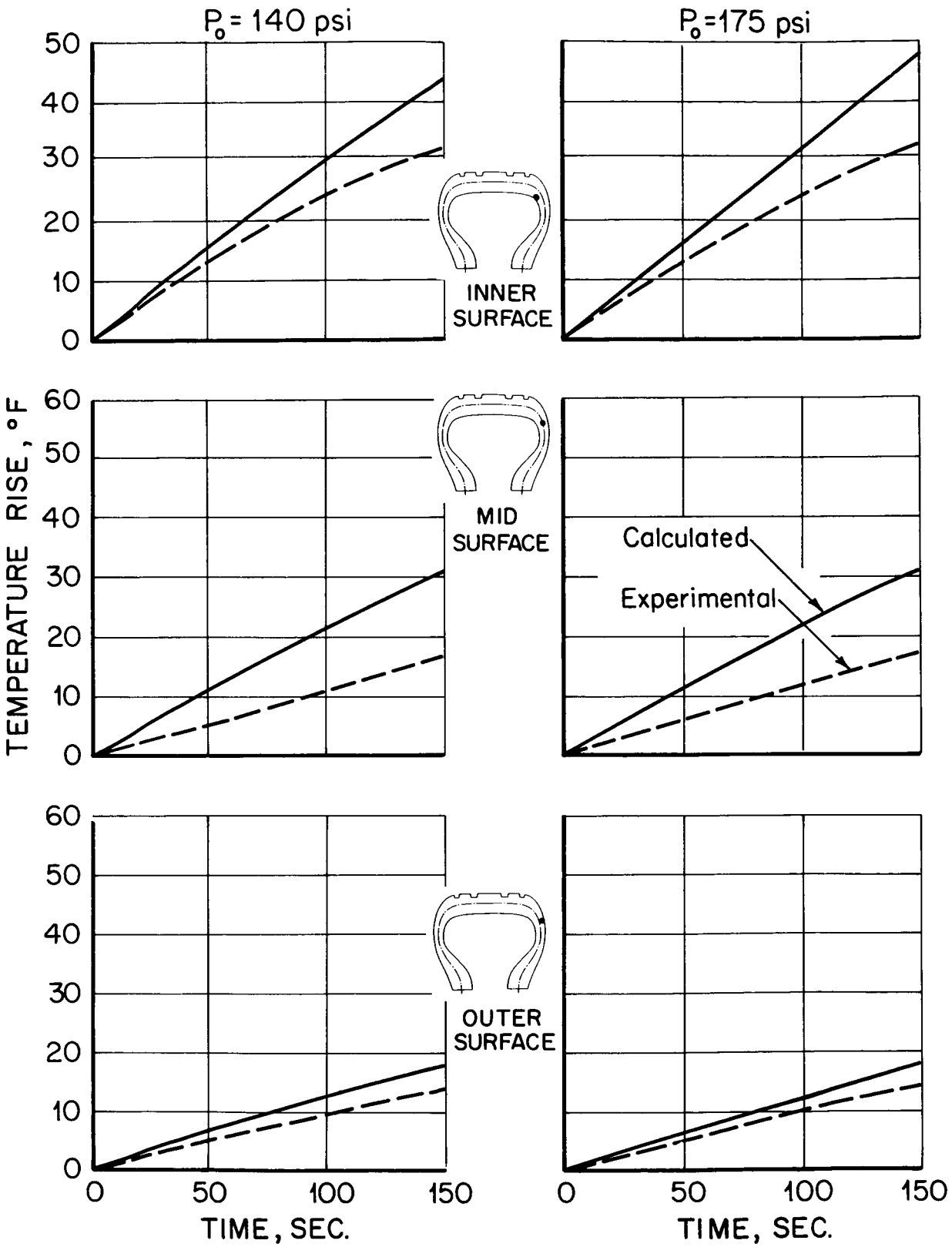

Fig. 31. Comparison of experimental and calculated temperature in upper sidewall region for yawed rolling for two different pressures. 40x14/22 PR, δ_z = 2.66 in., $\alpha = +3^o$, V = 20 MPH.

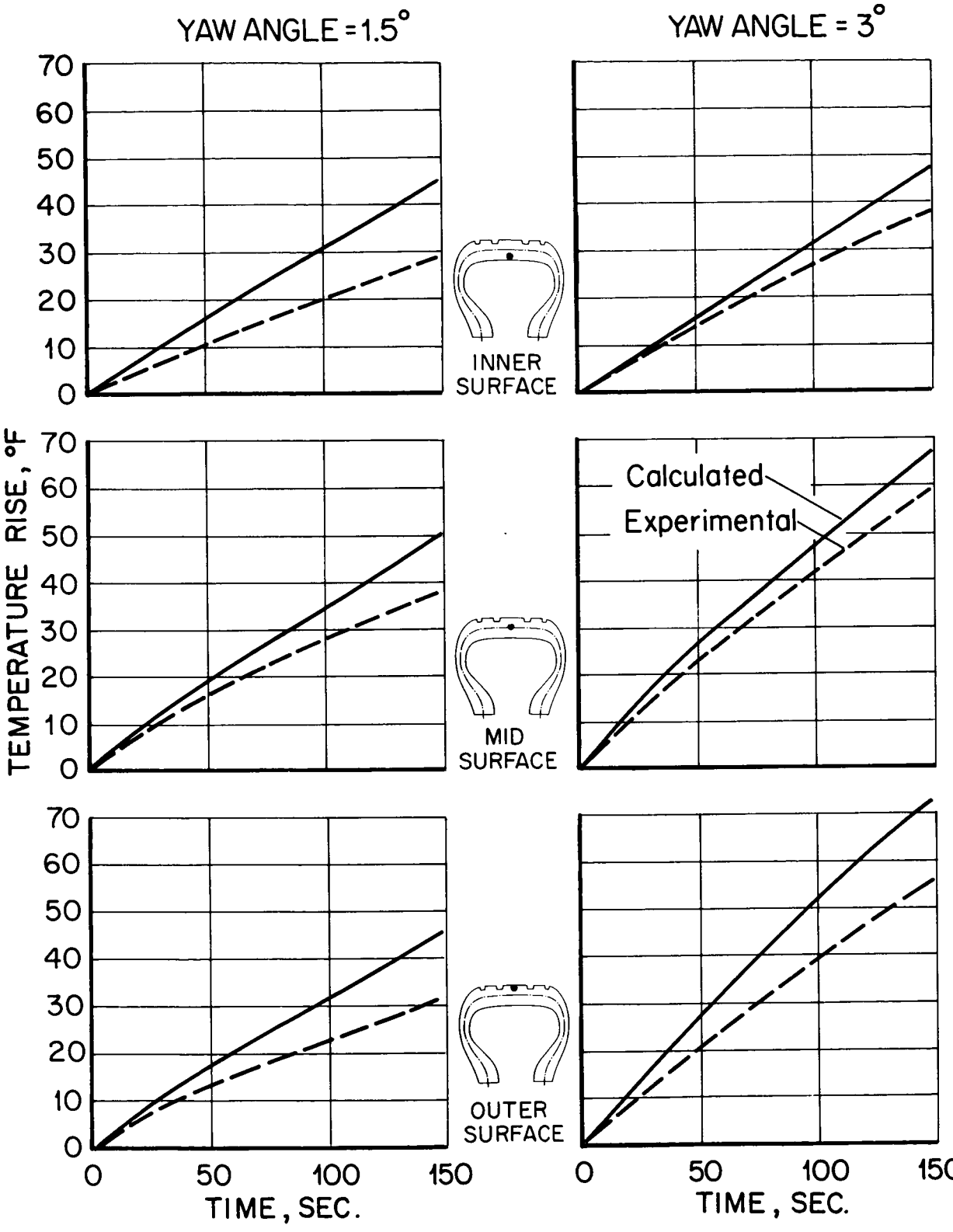

Fig. 32. Comparison of experimental and calculated temperature in the contact region for yawed rolling under two different steer angles. 40x14/22 PR, P_o = 175 psi, δ_z = 2.66 in., V = 20 MPH.

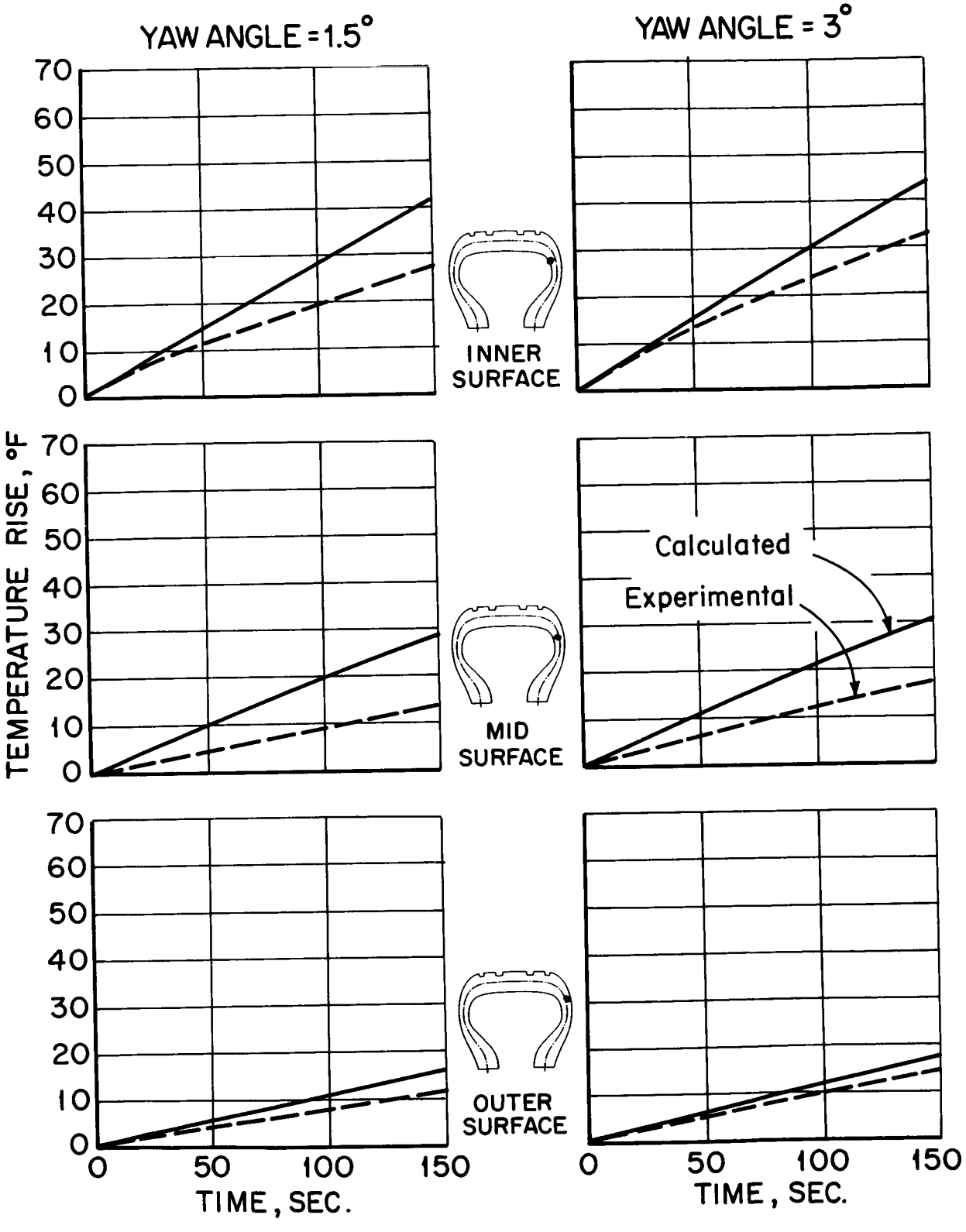

Fig. 33. Comparison of experimental and calculated temperature in the upper sidewall region for yawed rolling at two different yaw angles. P_o = 175 psi, δ_z = 2.66 in., V = 20 MPH.

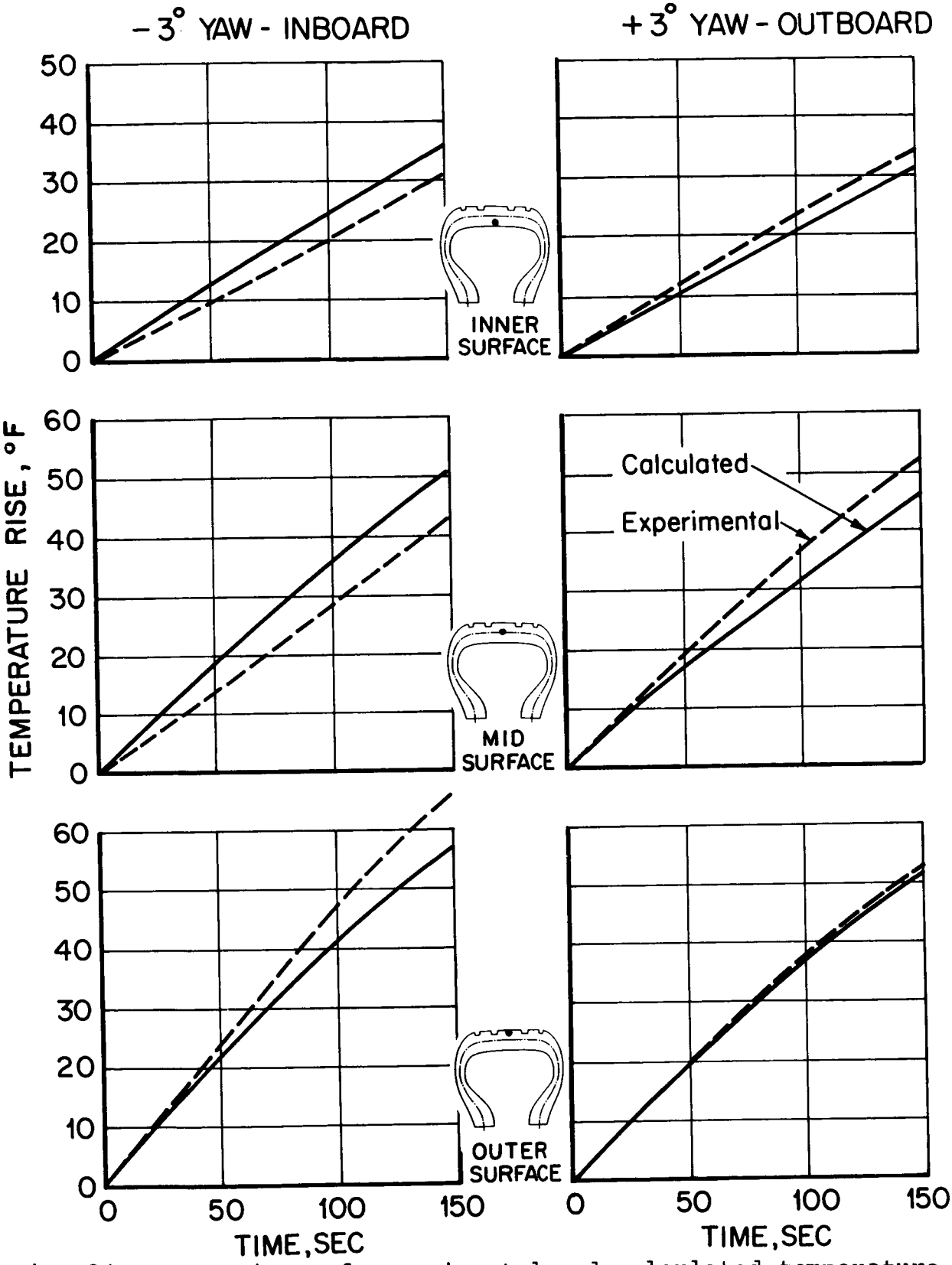

Fig. 34. Comparison of experimental and calculated temperature in contact region for yawed rolling for plus and minus 3° yaw. 40x14/22 PR, δ_z = 2.63 in., P_o = 140 psi, V = 20 MPH.

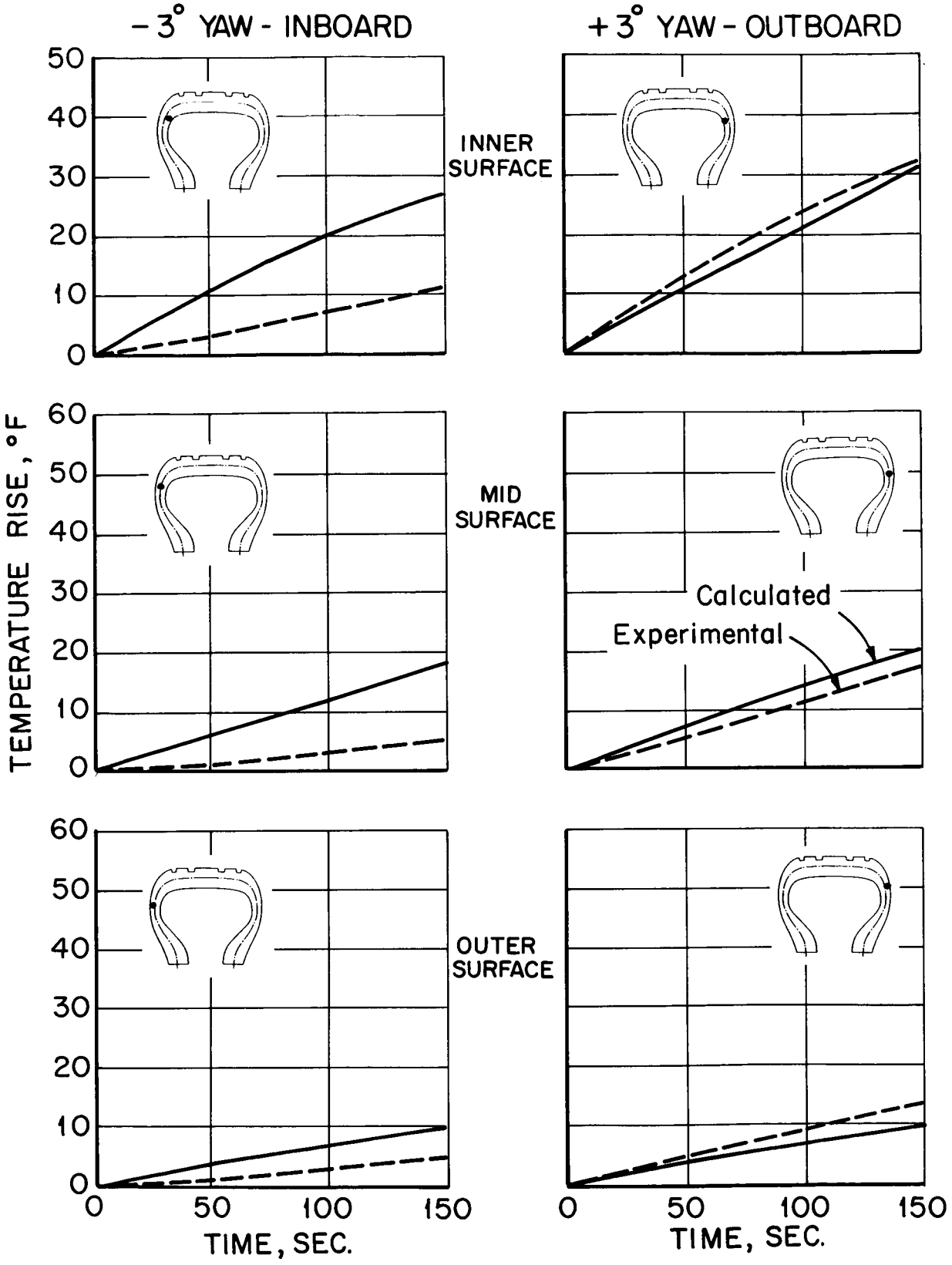

Fig. 35. Comparison of experimental and calculated temperature in upper sidewall region for yawed rolling for plus and minus 3° yaw. 40x14/22 PR, δ_z = 2.63 in., P_o = 140 psi, V = 20 MPH.

comparisons of individual locations in the carcass for various operating conditions. Secondly, they illustrate, as a function of time, the effect of the four operating parameters, tire deflection, tire inflation pressure, yaw angle, and direction of cornering on the temperature distribution for a fixed time.

Typical comparisons of experimental and calculated temperature changes in the contact and upper sidewall regions of the tire during yawed rolling are shown in Figures 28 and 29 for two different vertical deflections. As is observed from these figures, the temperature change predicted from the analytical model is in good agreement with the actual measurements. This is true for both the inside and outside portion of the tire as well as in the region out of contact.

A similar comparison for two different pressures is shown in Figures 30 and 31. Again the calculated results agree with the general trends although the overall comparisons with experiment are not as good as they were for variable deflection. This is especially true in the upper sidewall region where the calculations are consistently high.

Another such comparison for two different yaw angles is illustrated in Figures 32 and 33. Once again it can be observed that the general trends are represented by the analytical model.

Finally, in Figures 34 and 35, there is a similar comparison for both the inboard and outboard sides of the tire. Again the general trends have been predicted correctly but the overall correlations are not as good as previously. The predictions for the outboard side of the tire are closer to measured values than predictions for the inboard side.

CONCLUDING REMARKS

An analytical model has been developed for approximating the internal temperature distribution in an aircraft tire operating under conditions of yawed rolling. The model employs an assembly of elements to represent the tire cross-section and treats the heat generated within the tire as a function of the change in strain energy associated with predicted tire flexure. Special contact scrubbing terms are superimposed on the symmetrical free rolling model to account for the slip during yawed rolling.

An extensive experimental program was conducted to verify temperatures predicted from the analytical model. Data from this program were compared with calculation over a range of operating conditions, namely, vertical deflection, inflation pressure, yaw angle and direction of yaw. Generally the analytical model predicted overall trends well and correlated reasonably well with individual measurements at locations throughout the cross-section.

REFERENCES

1. Clark, S. K., Dodge, R. N.: "Heat Generation in Aircraft Tires Under Free Rolling Conditions". NASA CR-3629, 1982.

2. Clark, S. K., Dodge, R. N.: "Heat Generation in Aircraft Tires Under Braked Rolling Conditions". NASA CR-3768, 1984.

3. Smiley, R. F., Horne, W. B.: "Mechanical Properties of Pneumatic Tires with Special Reference to Modern Aircraft Tires". NASA TR R-64, 1960. (Supersedes NASA TN 4110.)

Standard Bibliographic Page

1. Report No.	2. Government Accession No.	3. Recipient's Catalog No.
NASA CR-4080		

4. Title and Subtitle	5. Report Date
Heat Generation in Aircraft Tires Under Yawed Rolling Conditions	July 1987
	6. Performing Organization Code
7. Author(s)	8. Performing Organization Report No.
Richard N. Dodge and Samuel K. Clark	
9. Performing Organization Name and Address	10. Work Unit No.
The University of Michigan Department of Mechanical Engineering Ann Arbor, MI 48109	505-63-41-02
	11. Contract or Grant No.
	NSG-1607
12. Sponsoring Agency Name and Address	13. Type of Report and Period Covered
National Aeronautics and Space Administration Washington, DC 20546	Contractor Report
	14. Sponsoring Agency Code

15. Supplementary Notes

Langley Technical Monitor: William E. Howell

16. Abstract

An analytical model has been developed for approximating the internal temperature distribution in an aircraft tire operating under conditions of yawed rolling. The model employs an assembly of elements to represent the tire cross-section and treats the heat generated within the tire as a function of the change in strain energy associated with predicted tire flexure. Special contact scrubbing terms are superimposed on the symmetrical free rolling model to account for the slip during yawed rolling.

An extensive experimental program was conducted to verify temperatures predicted from the analytical model. Data from this program were compared with calculation over a range of operating conditions, namely, vertical deflection, inflation pressure, yaw angle, and direction of yaw. Generally the analytical model predicted overall trends well and correlated reasonably well with individual measurements at locations throughout the cross-section.

17. Key Words (Suggested by Authors(s))	18. Distribution Statement
Aircraft Tires Tire Heating Yawed Rolling	Unclassified - Unlimited Subject Category 39

19. Security Classif.(of this report)	20. Security Classif.(of this page)	21. No. of Pages	22. Price
Unclassified	Unclassified	58	A04

For sale by the National Technical Information Service, Springfield, Virginia 22161